LA-UR-22-22709

Approved for public release; distribution is unlimited.

Title:	Additively Manufactured Tamper Evident Container (TEC)
Author(s):	Bernardin, John; Cattaneo, Alessandro; Gioia, Jack; Marchi, Alexandria; Mascarenas, David; Arinder, Graham; Juntunen, Aaron; Maki, Ryan; Meyerhofer, Peter; Rose, Alexander
Intended for:	Report
Issued:	2022-03-23

Additively Manufactured Tamper Evident Container (TEC)

Principal Investigator

John Bernardin

Co-Investigators

Alessandro Cattaneo, Jack Gioia, Alexandria Marchi,
David Mascarenas

Development Team

Graham Arinder, Aaron Juntunen, Ryan Maki, Peter Meyerhofer, Alexander Rose

Los Alamos National Laboratory

March 21, 2022

Table of Contents

1.0 Project Introduction and Technology Demonstration Motivation

The protection of sensitive data, proprietary information, and physical assets from adversarial disclosure is a high priority in today's environment of government and industrial espionage. Furthermore, knowledge of the security history and monitoring for potential acquisition or disclosure of the protected assets from oppositional sources is equally important. In 2016, as part of an LANL Institute for Materials Science (IMS) rapid response research initiative, the investigators of this technology demonstration project developed the concept of an additively manufactured tamper resistant container that possessed tamper evident features. Tamper evident seals and detection technologies have a long history in protecting consumers from product tampering, recording the installation and activation of mechanical safety panels and fasteners on dangerous electro-mechanical systems, and serving as a warranty void indicator on expensive electronic equipment. Examples of such tamper evident seals range from "no-tech" versions, e.g., the paper seals under medicine caps, to "high-tech" seals that are radio frequency-active and include encryption capabilities used by the International Atomic Energy Agency (IAEA) to monitor stored nuclear materials in support of safeguards missions. The tamper evident container (TEC) technology would have many uses including the following examples:

1. Serving as the transportation and encrypted monitoring cases for weapon components or systems between the production facilities and assembly or deployment centers, or vice versa.
2. Providing surety packaging of captured or retrieved radioactive sources or materials for shipment to a protected collection facility.
3. Transportation of sensitive information, technology, software, or physical articles between facilities or work sites.
4. Protection and surety of critical assets under storage.
5. Incorporating engineered-controlled defensive measures to protect or destroy container-protected assets.

A demonstration TEC, shown in Figure 1.1, was produced as part of the IMS study using advanced Additive Manufacturing (AM). AM allowed for the insertion of uniquely patterned conductive plastic traces within the walls of a non-conductive plastic container. An integrated analog circuit was designed to track the continuity of the traces and provide a latched trigger signal if one or more of the traces, and hence container walls, was violated. In concept (i.e., not yet constructed), a small digital computer with an RF transmitter would monitor the trigger signal and provide for other diagnostic resources such as GPS tracking, environmental monitoring (e.g., temperature, pressure, vibration, humidity, etc.) as well as communication to an exterior monitoring station. Both the pattern of the conductive traces in the container and the digital key for accessing the TEC monitoring system would be encrypted for enhanced security. That was the extent of the IMS project which concluded in 2017 and a fully integrated and functional unit was not developed.

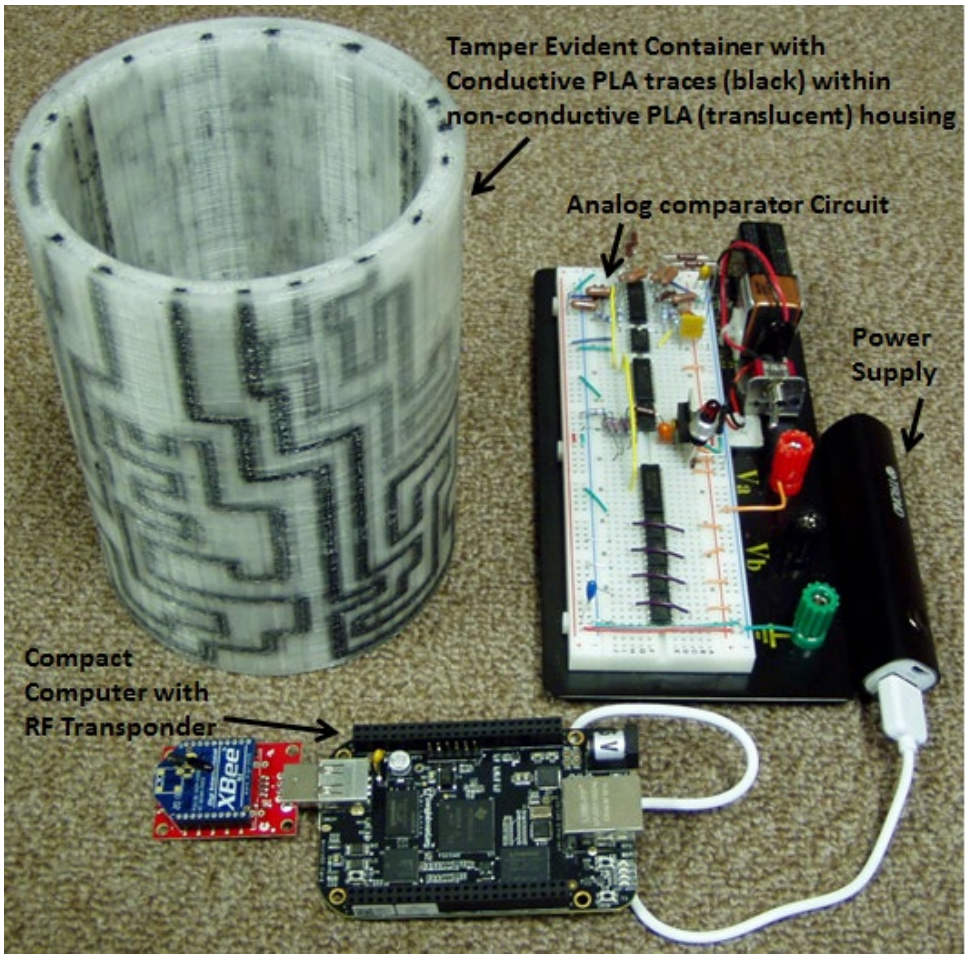

Figure 1.1. Prototype Tamper Evident Container including analog and digital electronics. In 2018 a provisional patent of the Tamper Evident Container (TEC) technology was submitted by Los Alamos National Security and in 2019, a follow-on full patent application was filed by Triad National Security to the US Patent Office.

The submission of the patent application motivated the investigators of the current study to build off of the previous TEC concept and develop several fully functional prototype units. The demonstration units would be used to showcase the technologies developed or harnessed by LANL to advertise TEC capabilities and showcase implementation strategies for weapons, global security, and information security programs as well as a number of other defense and commercial applications. Furthering the development of the TEC demonstrators could also assist the developers in securing funding to mature the technology and manufacturing readiness levels to make the end-products more realizable.
This motivation lead to the formation of the following goals which were proposed as part of this technology demonstration project:

- Fabricate a demonstration prototype TEC and associated electronics. The system will be mounted in portable and protective display case to allow it to be transported and used as an exhibition unit.
- Provide one unit with both basic tamper evident functionality and advanced functions for environmental monitoring, location tracking, and defensive posturing. This unit will

demonstrate the versatility of this technology in accommodating varying asset geometries and end uses.

- Provide a communication system to transmit the container integrity status, environmental parameters, and location information to a computer network. Compressive sensing encryption strategies will be applied to this communication system.
- Identify end-users of the TEC technology and establish lines of funding to produce fully functional and deployable designs for numerous applications.

As this technology demonstration project progressed, the team decided to modify the goals and to focus on the tamper evident technologies and manufacturing methods and to not construct the functions for environmental monitoring, location tracking, and defensive posturing. It was felt that the tamper evident technologies were the heart of the patent and needed to be demonstrated, whereas the other functions were well developed and could be easily incorporated at a later time. As will be shown in the following sections of this report, two functional TEC units were fully developed and tested, each with a different sensing and monitoring scheme (electrically conductive traces versus fiber optic traces). The conductive trace sensing TEC was constructed from a previous design concept of the research team. In this present case, a newer technology 3D FDM printer with some improved dual material printing capabilities, was employed to improve the formulation of the conductive traces within a non-conductive wall. The fiber optic sensing TEC resulted from the integration of several technologies that when combined, are novel and are being considered for a provisional patent application. A third sensing scheme that utilized mechanical vibration propagation was explored but finite time and resources prevented the team from building a demonstration unit of that technology.

The remaining sections of this report describe the TEC design requirements, the mechanical design and additive manufacturing methods used to build demonstration units, the design and construction of the analog and encrypted digital electronics required to drive the TECs, and the physical details of the integrated TECs as well as the corresponding test results.

2.0 TEC Design Requirements

To guide the TEC team in constructing functional technology demonstration units, the following functionality and performance requirements were defined.

1. The TEC shall serve as a demonstration unit for conveying purpose and functionality of the associated technologies and thus will not be optimized for pure performance (i.e., TEC features may be purposely visible for demonstrating manufacturing technique).
2. The TEC shall monitor for, detect, record, and alert TEC owners of an adversary attempting to or succeeding at gaining access to the container to view, probe, handle, or gain access to the protected object.
3. The TEC does not have to act as a "safe" to prevent access to the object.
4. The TEC does not have to provide any defensive measures should an adversary gain access to the object.
5. The TEC shall be capable of holding a solid object (rough size 2"x2"x3", max weight = 3 lbf), and prevent direct visual access of the object when the TEC is in a closed configuration.
6. The TEC shall have an electrical/software capability that monitors and records the integrity of the container on either a continuous or a random basis.
7. Each TEC of a given sensing technology shall be unique in both its mechanical and electrical/software designs.
8. The TEC mechanical design shall be have features that deter replication or counterfeiting.
9. The TEC electronics/software shall be encrypted to prevent tampering with or counterfeiting the system.
10. The TEC mechanical design shall have the features to detect an adversary attempting to gain access to the protected object by the following means:
    a. Mechanical insult: drilling, cutting, debonding, and tearing.
    b. Chemical insult: burning, melting, dissolving

To make the TEC development units more realizable with the time, budget, and resource constraints, the following design requirements were defined.

11. The TEC shall operate off of two commercial 9VDC batteries for the electronics which may be rechargeable or replaceable.
12. The electrical power source shall be contained within the TEC along with all analog and digital electronics required by the prototype(s).
13. The TEC shall operate on a continuous basis for up to 3 days when fully charged, or on a random monitoring basis for up to 7 days when fully charged.
14. The TEC shall not have any power nor communication ports that cross the outer mechanical boundary of the TEC. All communication and power transmittal ports will be located directly on the electronic elements inside the TEC.
15. The TEC shall have a USB 3 communications port for accessing the digital electronics (no wifi nor Bluetooth)

The TEC shall use embedded sensing on the external container walls to provide for monitoring of the TEC. Every attempt will be made to use AM to produce the mechanical container and to create or embed the sensing in the container walls.

3.0 Conductive Trace (CT) TEC

3.1 Basic Construct of CT-TEC

As mentioned previously, the CT-TEC design was an artifact of a previous IMS research project. The basic container design, shown in Figure 3.1 was utilized in this technology demonstration project with a few critical improvements. Resulting from the previous IMS funds, partially successful CT-TECs were printable with many limitations because of the 3D printing technology at that time. The open-sourced FDM printer, a Lulzbot Taz, had many problems printing the conductive plastic, including filament leaking from the nozzle, filament breaking in the extruder assembly, smudging, and low resolution in printed trace thicknesses. These problems limited printability and reduced design flexibility that is normally where additive manufacturing processes excel. Advances in commercial technologies since the prior IMS research have improved the printability of the conductive traces inside non-conductive plastic, providing significant flexibility in how the CT-TEC may be designed and printed. These advances, now available in the Ultimaker shown in Figure 3.2, include the following: 1) greater printing resolution (20 μm vs. 100 μm on the Taz), 2) more software control features around printing process, 3) more forgiving extruder to handle the brittle conductive filament, 4) an adjustable dual-extruder that lifts the conductive filament nozzle up when not printing to reduce smudging and ultimate shorting between traces. These advancements in commercial technology allowed repeatedly successful prints of the previous CT-TEC design and provides significant flexibility for more robust designs in the future.

Figure 3.1 CAD model of the CT TEC showing the electrically non-conductive mechanical housing and the electrically conductive traces in the housing walls. Lid latching mechanism and inner analog and digital electronics omitted for clarity.

Other new features in this CT-TEC version include a latching lid with more robust electrical connections and an inserted mounting box to house the analog and digital PCBs along with the batteries. These features are described further in the following sections.

3.2 Mechanical Housing

3.2.1 CT TEC Main Housing and Conductive Traces

The CT TEC mechanical housing, shown previously in Figure 3.1, was 3D printed from two materials simultaneously on an Ultimaker S5 FDM machine, shown in Figure 3.2. The Ultimaker S5 was chosen for its high resolution (20 μm in layer and 7 μm in horizontal), repeatable printing capabilities, as well as its open source format which allowed the researchers to adjust the nozzle feed and temperature settings to best match the needs of the plastic filament material used in this demonstration study.

Figure 3.2. Ultimaker S5 FDM 3D Printer with dual nozzle assembly.

For the demonstration unit, transparent PLA was chosen as the main housing body material. PLA was chosen for several reasons. First, its print settings are compatible with the print settings of the conductive PLA used in the traces. Second, PLA prints very reliably, which was important due to the length and complexity of the print as well as the temperamental nature of the conductive PLA. Third, transparent PLA was chosen so that the traces could be seen in the demonstration unit. The production units of the container would use a non-transparent material to visually obscure the location of the traces. A material other than PLA could also potentially be chosen to increase the durability of the container.

The second material is Proto-pasta conductive PLA. This material is a compound of PLA, which is non-conductive, and carbon black. It is a fairly high resistance material with a reported volume resistivity of 115 Ω*cm in the z (vertical) direction; for comparison, copper has a volume resistivity of 1.68*10^-6 Ω*cm. This material can be fairly challenging to print for several reasons. First, the filament is prone to clogging in nozzle and having the material strip in the extruder assembly. When a filament strips, the extruder gear grinds into the filament instead of

pushing it, and the filament stops extruding since there is nothing pushing it. The material is also prone to oozing out of the nozzle when it is not printing which can cause interconnections between the traces. Some of these challenges were overcome by the use of the Ultimaker S5. The Ultimaker S5 has a sensor that can recognize a lack of material flow and pause the printer. This prevents printing a container where there are no traces due to a material clog. The dual extrusion mechanism on the printer lifts the nozzle that is not printing above the part. This action helps prevent the resulting material oozing from the non-printing nozzle (i.e. conductive material) from making interconnections between traces.

The print settings that were used on the Ultimaker S5 to produce the conductive trace TEC are given below.

General Print Parameters

- Infill: 100%
- Layer Height: 0.2mm
- Wall Layer Count: 3
- Nozzle Filament Control: Retract filament when traveling
- Nozzle Control: Z-hop when traveling

Nozzle Print Core 1: CC- 0.6mm ruby tipped nozzle

- Material: ProtoPasta Conductive PLA-2.85mm
- Temperature: 210 °C
- Speed: 30 mm/s
- Fan: 100%

Nozzle Print Core 2: AA-0.4mm brass nozzle

- Material: Matterhackers Natural PLA-2.85mm
- Temperature: 200 °C
- Speed: 70 mm/s
- Fan: 100%

The conductive PLA is printed hotter and slower than PLA as it is more viscous when melted due to the added conductive material. It was found that printing the material slowly led to a higher quality print. The hotter print temperature, compared to PLA, helps ensure good adhesion between layers which leads to better conductivity. A ruby tipped nozzle was used for the conductive PLA because it is an abrasive filament.

3.2.2 Latching Mechanism

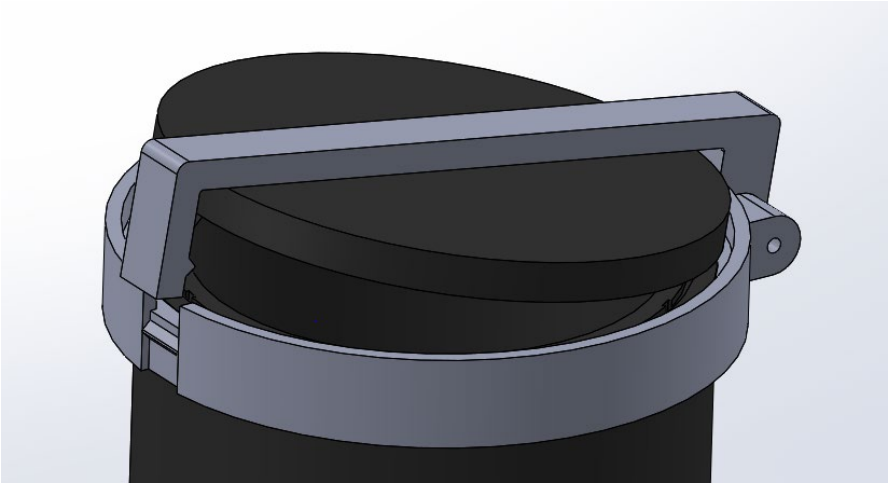

Figure 3.3. Latching mechanism CAD model for the CT TEC.

The latching mechanism design shown above in Figure 3.3, was inspired by the flexible plastic latches common on everything from electronics closures to backpack buckles. It is made up of two components including a collar that slips around the container and a bale that secures the lid to the container. The rear of the latch mechanism pivots on hinge, while the front uses the buckle inspired design that was mentioned previously. The collar and the bale have triangular protrusions that interfere when closing the lid. Some force is required to flex the two protrusions past each other. Once the two protrusions have passed each other, the container is latched and holds the lid with enough force to make the electrical connections between the container body and the lid. The latch helps to sandwich a one-directional highly conductive Zebra strip to electrically bridge between the conductive pads on the body and lid. This latch was designed for the demo unit so that the lid could be opened and closed easily to show how the container reacts to the electrical connections being broken. This closing mechanism will be redesigned for production units to offer a more secure closing mechanism.

3.2.3 PCB Holder

The electronics holder for the conductive trace TEC (see Figure 3.4) was designed with the intent to use additive manufacturing (AM) as the production method. When designing for AM, the goal is to have as few overhangs and roofs that require support as possible. For this electronics holder, it was possible to entirely avoid using support material. To design the holder, first a half cylinder with a radius matching the interior radius of the TEC was extruded. Next, a sketch was made on the top surface of the cylinder. This sketch had two primary purposes, first to provide the mounting grooves that the board slots into and second to provide clearance for board components to fit into the interior of the cylinder. This sketch was cut into the cylinder to a depth that matched the length of the board, making sure to leave a bottom on the container. Finally, a sketch was made on the top surface to create a mounting tube for the two 9V batteries that power the container. This sketch was cut into the container to a depth that matches the height of the two batteries. Once the design was finished, the electronics holder was 3D printed in ABS plastic on a Stratasys F370.

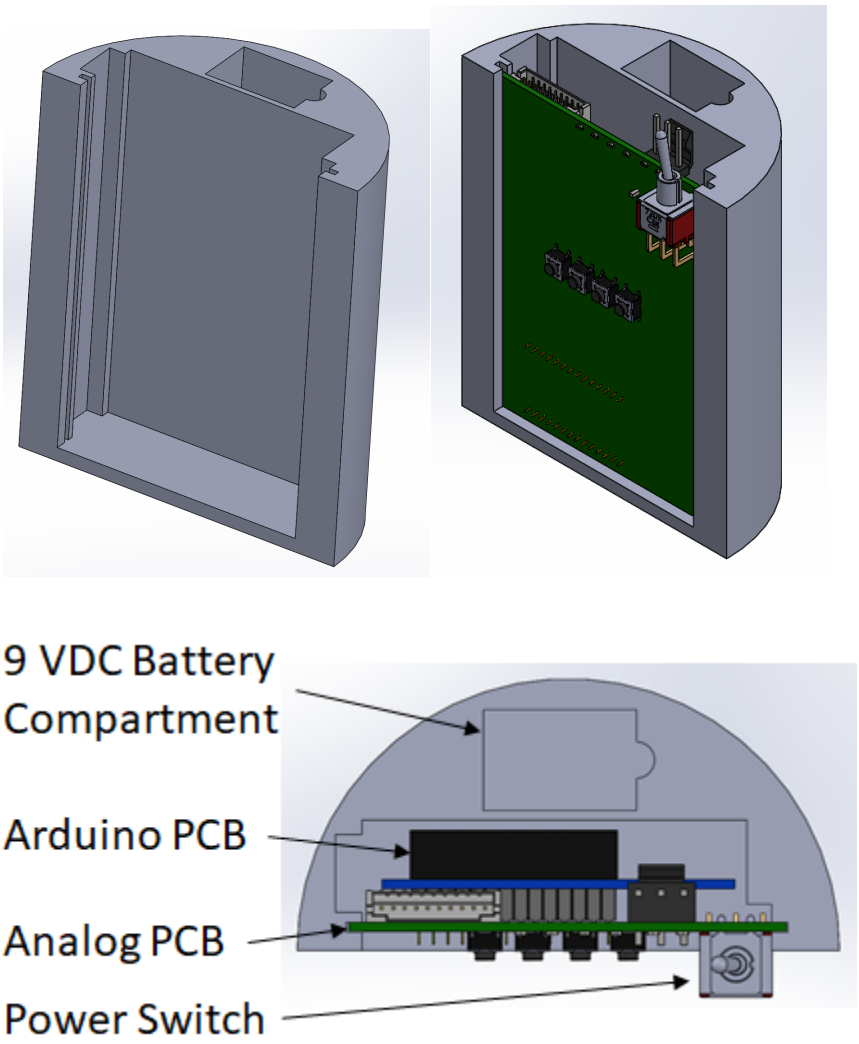

Figure 3.4 CAD model of the mechanical holder for the analog and digital PCBs and batteries and the integrated electronics.

3.3 **Analog Electronics**

The analog electronics concept for the conductive trace tamper proof detection was based on discreet logic gates and analog circuitry. The tamper proof construction was fabricated using a uniquely patterned conductive plastic traces within the walls of a non-conductive plastic container. To detect a fault in the conductive plastic traces an analog front end was designed. Comprising the analog front end input detection is a LM331 single comparator circuit configured as a negative acting level detector. Originally a quad comparator was chosen (LM339) as to handle 4 sides (quadrants) of a container or other shipping configuration but it was decided to change that to single comparators to isolate any one particular channel failure fault. The digital and analog information is fed to a Central Processing Unit (CPU) that is attached to the digital/analog Printed Circuit Board (PCB). Refer to schematic 63Y-1773785, shown in Figure 3.5.

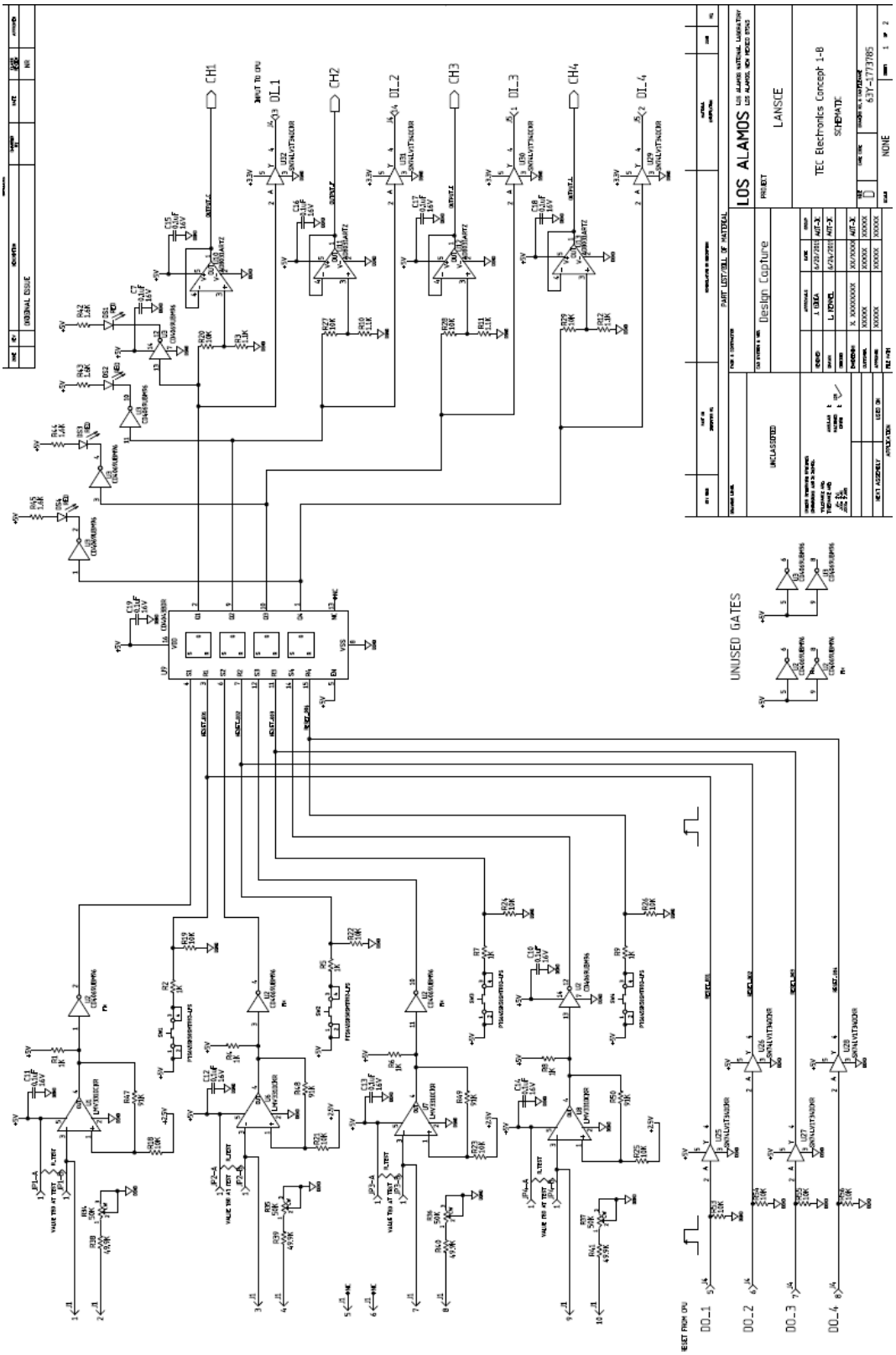

Figure 3.5. Analog electronics schematic for the conductive trace TEC.

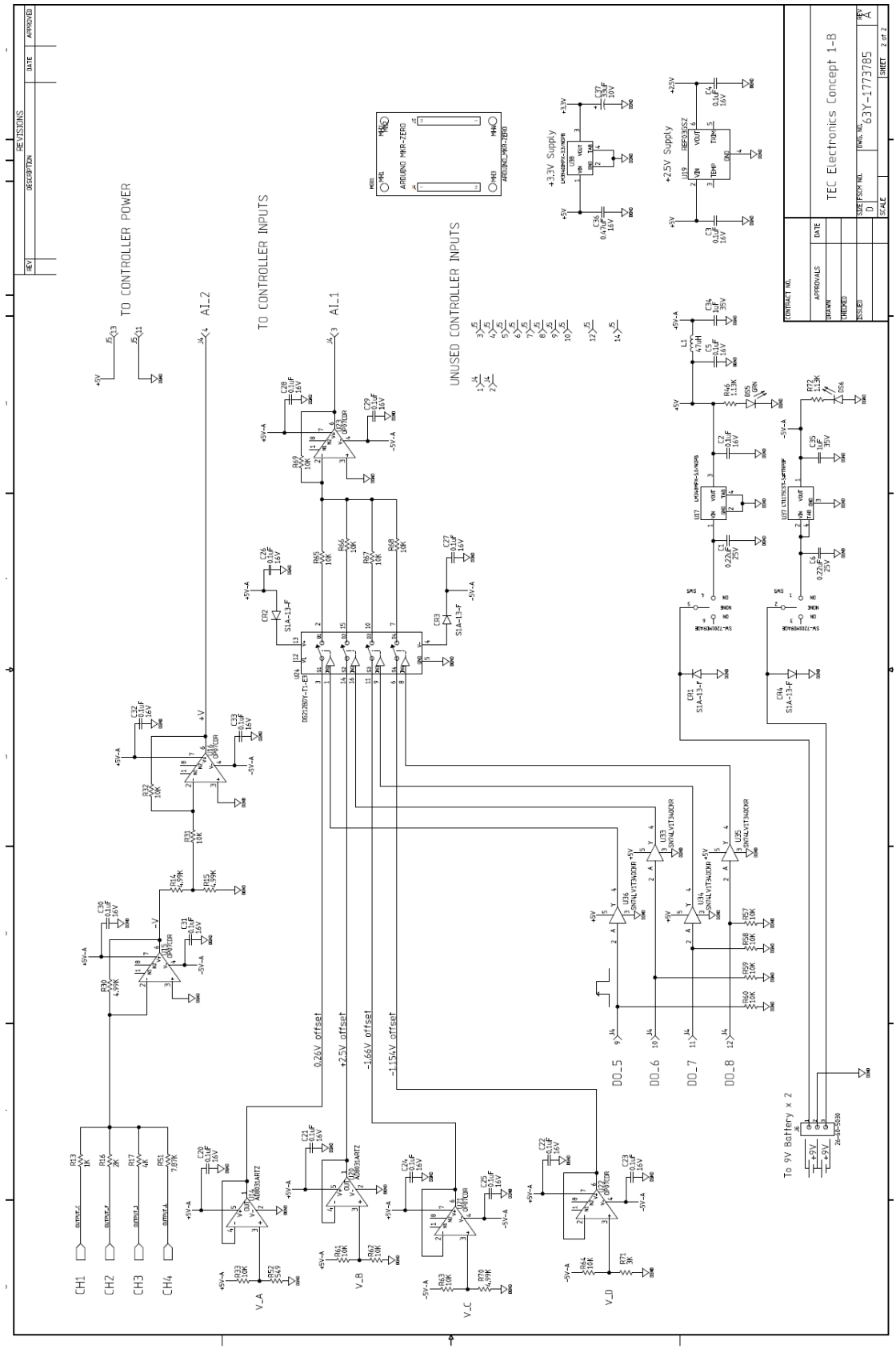

Figure 3.5 – continued.

A +2.5V reference is feed to the + terminal of each comparator, positive feedback is employed to achieve hysteresis around the input. The – terminal is pulled high to +5V with a resistor to balance the conductive trace resistance in a particular quadrant. The output terminal of the comparator is pulled high with a resistor and will trigger low upon a faulted input condition. By using a resistance ratio of the – terminal to the quadrant resistance network resistance, say of a 4 sided container, we establish a voltage level at that comparator terminal. As long as the voltage at the – terminal is below the +2.5V reference voltage the output of the comparator is not triggered and remains high. Once triggered the output will go low and set the R/S latch. Even if the breach is back to normal the latch will report a breach condition until reset by the CPU. We are using an Arduino CPU for this demonstration.

We have incorporated a second digital/analog circuit to add a voltage offset to a second Arduino CPU analog input. We can change the 4 bit digital coding to establish an offset voltage associated with a particular breach condition or set a bit to send a voltage which is polled at to indicate the system is operational and that the power supply voltages are OK . This circuit has to be modified as the Arduino CPU chosen at this time cannot handle negative voltages. This detector method was chosen so we could always monitor voltage present for the system or enable a bit to random sequence a voltage as an additional safeguard for tamper protection of the PCB electronics. Also using a Watch Dog timer approach we can monitor the input voltage polling and ensure suitable voltage is present for proper system operation and offset voltage is predicated based on the digital commend the CPU send out to the digital/analog PCB.

Upon tampering of the quadrant resistor network, breakage, sanding or cutting some of the embedded container network, would cause the container resistance to go “open” or into a high resistance state, the negative terminal would go above +2.5V threshold and trigger the comparator output. This will latch on any of the four quadrant attacks even if the breach is restored by a temporary or permanent repair.

Once triggered, the signal is now in digital format and goes to an inverter to invert the level to +5V. The +5V is feed into an R/S latch. The output of the latch will remain until reset by a reset signal sent by the control system.

The latched quadrant +5V signal is then stepped down to approximately 0.26V and sent to a summing analog amplifier. The output of the summing amplifier is then sent to the CPU and a weighted summing amplifier amplifies the voltage and shown as some typical examples in the digital decoding tables. By establishing different gains for each of the quadrants we can determine which quadrant has been compromised with an analog voltage as second verification. We also have this with the 4 digital inputs which are activated by the breached section. Using binary 4 bit truth table we can double verify which quadrant has been breached.

One can see from the tables that different weighting functions can be used to produce different analog voltages. This makes it difficult for a perpetrator to figure out the decoding scheme.

Refer to Table 3.1, Decode Method 1, where we have assigned weighted values and produce different voltages that are fed to the summing amplifier producing the outputs shown.

Refer to Table 3.2, Decode Method 2, where we have reversed the assigned weighted values and produce different voltages that are fed to the summing amplifier producing the outputs shown.

Table 3.1. Decode Method 1.

TEC Digital weighted decoding methodology with Analog Voltage

Base 10	Weighted Input D (8)	Weighted Input C (4)	Weighted Input B (2)	Weighted Input A (1)	-Output Voltage from summing amplifier with weighted inputs (V	Divide by 2 and invert signal to DPU (V)
0	0	0	0	0	0	0
1	0	0	0	1	-0.15625	0.078125
2	0	0	1	0	-0.3125	0.15625
3	0	0	1	1	-0.46875	0.234375
4	0	1	0	0	-0.625	0.3125
5	0	1	0	1	-0.78125	0.390625
6	0	1	1	0	-0.9375	0.46875
7	0	1	1	1	-1.09375	0.546875
8	1	0	0	0	-1.25	0.625
9	1	0	0	1	-1.40625	0.703125
10	1	0	1	0	-1.5625	0.78125
11	1	0	1	1	-1.71875	0.859375
12	1	1	0	0	-1.875	0.9375
13	1	1	0	1	-2.03125	1.015625
14	1	1	1	0	-2.1875	1.09375
15	1	1	1	1	-2.34375	1.171875

Notes:

1) a separte analog circuit sends an offset voltage of +0.26V to a second DPU analog input (0.25V used for calculations)
2) each "1" represents one of 4 container breachs and or combinations of each
3) D is most likely; A is least likely breach
4) weighted voltages: D=1.25V; C=0.625V; B=0.3125V; A=0.1563V

Table 3.2. Decode Method 2.

TEC Digital weighted decoding methodology with Analog Voltage

Base 10	Weighted Input D (8)	Weighted Input C (4)	Weighted Input B (2)	Weighted Input A (1)	-Output Voltage from summing amplifier with weighted inputs (V	Divide by 2 and invert signal to DPU (V)
0	0	0	0	0	0	0
1	0	0	0	1	-1.2500	0.625
2	0	0	1	0	-0.625	0.3125
3	0	0	1	1	-1.875	0.9375
4	0	1	0	0	-0.3125	0.15625
5	0	1	0	1	-1.5625	0.78125
6	0	1	1	0	-0.9375	0.46875
7	0	1	1	1	-2.1875	1.0938
8	1	0	0	0	-0.15625	0.078125
9	1	0	0	1	-1.4063	0.70315
10	1	0	1	0	-0.7813	0.39065
11	1	0	1	1	-2.0313	1.01565
12	1	1	0	0	-0.4688	0.2344
13	1	1	0	1	-1.7188	0.8594
14	1	1	1	0	-1.0938	0.5469
15	1	1	1	1	-2.3438	1.1719

Notes:

1) a separte analog circuit sends an offset voltage of +0.26V to a second DPU analog input (0.25V used for calculations)
2) each "1" represents one of 4 container breachs and or combinations of each
3) A is most likely; D is least likely breach
4) weighted voltages: A=1.25V; B=0.625V; C=0.3125V; D=0.1563V

The weighted voltage values can be arranged to produce a unique voltage that would be difficult to decode without prior knowledge of the decode scheme.

In addition, by having the weighted analog voltage and the offset analog voltage we can process the information with a fast Analog-to-Digital Converter (ADC) and send various messages wirelessly to receiving stations or central communication networks.

3.4 **Digital Electronics & Software**

The CT TEC demonstration unit is equipped with a single board microcontroller Arduino model MKR ZERO. The MKR ZERO board was chosen to meet several CT TEC requirements. The TEC unit is powered on a battery and operates continuously over the long term. For this reason, the digital board must feature low power consumption. The MKR ZERO board is equipped with

a low power microcontroller. Lab measurements showed that the MKR ZERO board, which operates at a voltage of 3.3 V, has the power requirements listed in Table 3.3. Additional comments on the energy consumption and projected battery duration are provided in the following section.

Table 3.3. Arduino MKR ZERO electrical current and power requirements.

Status	*Current*	*Power*
Initialization	18 mA	59.4 mW
Idle	1 mA	3.3 mW
Check status / Alarm report	10 mA	33 mW

The MKR ZERO board provides additional desirable features. With a size of only 6 in x 2.5 in x 1 in, it fits easily inside the TEC unit. It also has an on-board SD connector that enables it to write data on a micro-SD card. Importantly, the MKW ZERO board is equipped with 22 digital input pins, 7 analog input pins (with a 12 bit analog to digital converter, ADC) and 1 analog output pin (with a 10 bit digital to analog converter, DAC). The input/output pins provide plenty of capability to interface the Arduino with the analog electronics described in Section 3.3. Figure 3.6 shows the schematic of the connections between the Arduino and the analog circuitry board.

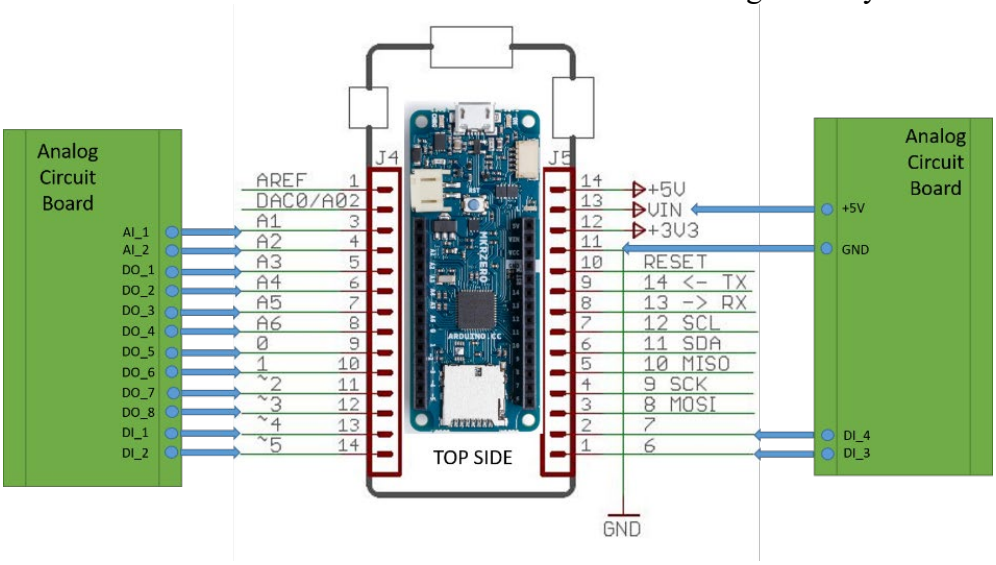

Figure 3.6. Schematic of the connection between the analog circuit board and the Arduino MKR ZERO.

The Arduino is programmed to reset the analog circuitry board and continuously monitor the CT TEC unit's health status by reading the digital and analog outputs of the analog circuitry board. Further, the Arduino provides the TEC unit with data encryption features. Encryption is used to authenticate the TEC unit and protect the data written on the SD card. Arduino's operation and encryption details are provided in Sections 3.4.1 and 3.4.2, respectively. Further, Section 3.4.3 shows how the Arduino's operation and encryption are used in the CT TEC demonstration.

3.4.1 CT TEC Arduino's operation

The Arduino installed on the CT TEC was programmed to operate as follows:

1. Upon pressing a switch on the analog circuitry board, the Arduino powers up and does not perform any operation during a predetermined interval of time (e.g. 30 seconds) to allow for the CT TEC's lid to be closed.
2. Once the waiting time has elapsed, the Arduino initializes the input/output pins configuration. It also resets the latches on the analog circuitry board that were initially triggered by the lid being open.
3. The SD port is initialized to enable the Arduino to write data on the SD card. At this point, the Arduino checks that an SD card is present in the SD slot. If the SD port initialization fails or an SD card is not detected, the Arduino aborts any subsequent steps;
4. The real time clock (RTC) is initialized. This operation is necessary to allow for the use of the encryption algorithm.
5. The encryption algorithm is initialized. At this point, the Arduino is ready to write encrypted messages on the SD card.
6. The Arduino starts to continuously monitor the TEC status. The Arduino enters the idle mode that is characterized by minimum power consumption. There are only two events that can wake up the Arduino from the idle mode: (1) a latch on the analog board is triggered by a tampering event; (2) an ad-hoc function wakes up the Arduino and forces it to write an encrypted message on the SD card at constant intervals of time. The wake-up function has been created to periodically verify that the Arduino is working. Writing encrypted messages on the SD card at regular interval of times enables one to understand when the Arduino successfully woke up last. This information can be used for diagnostic purposes as it enables one to verify that the battery was still supplying energy to the unit at that time.

The flow chart presented in Figure 3.7 helps to visualize steps 1-6. The flow chart shows that the Digital Input (DI) Interrupt can be triggered when one of the digital pin on the analog circuitry is set off by a tampering attack. When the DI Interrupt is triggered, the Arduino interrogates the RTC clock, measures the analog input (AI) voltages from the analog circuitry board and interrogates the status of analog circuitry board's digital input (DI) pins. The data collected are used to update the variables used in the Arduino code and an encrypted message is written on the SD card. The same stream of events generated by the DI Interrupt being triggered, can be initiated by the wake-up function used to periodically check the Arduino's status.

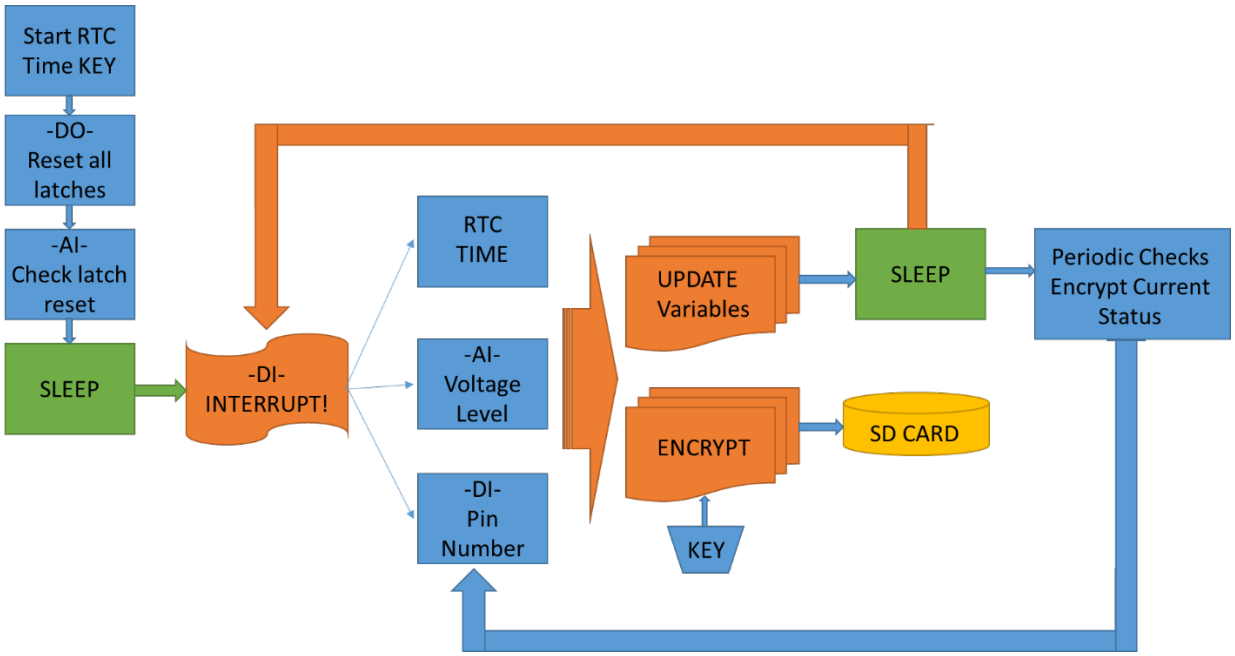

Figure 3.7. CT TEC Arduino's operation flow chart

3.4.2 CT TEC Encryption

The Arduino's community has developed libraries to implement a number of commercial encryption algorithms. For this specific project, the ChaCha20-Poly1305 AEAD was chosen as it is largely recognized as the best cipher for mobile applications in terms of performance (i.e. speed) and security. The cipher consists of two main parts: plain text and encrypted text. The plain text contains a time stamp (i.e. elapsed time since the real time clock has been started up) and an initialization vector (i.e. a 12-byte random number). The encrypted text is a message of predefined length that protects sensitive data from being disclosed to an unauthorized third party. The Arduino installed inside the CT TEC unit uses the ChaCha Poly algorithm to record the following encrypted message on the SD card: why the message was generated (alarm or periodic check), time when the message was created, and state of the 4 digital pins and 2 analog pins on the electronic circuitry board. Figure 3.8 shows how the original message looks like before and after it is transformed into a cipher.

```
D31A8D34648E60DB7B86AFBC53EF7EC2A4ADED51296E8FEA9E2B5A736EE62D63DBEA45E8CA9671282FAFB69DA92728B1A71DEA9E6B295D  <-Encrypted HEX
§□¶4d§`§{§§§s§~u§§Q)r□§§□6%b§=§§^§§g□§§§i jr§□q§                                                                <-ASCII representation of
§□□)□§~§;6§µ ~w§§§□§§({□x§§$§§§u§u§§§§H1□?§§§§Kz§§v§e§§§Ka□                                                      encrypted text
4C6164696573206166420476566746C656D656B206F662074686520636C617373206F66202739393A204966204920636F756C64206F66  <-Decrypted HEX
Ladies and Gentlemen of the class of '99: If I could offer you only one tip for the future, sunscreen would be  <-ASCII of decrypted text
```

Figure 1.8. Example showing the original message content and the associated cipher

3.4.3 CT TEC Demonstration

The CT TEC's demonstration required the programming of 2 separate Arduinos. One Arduino was installed inside the CT TEC unit and it was used to save an encrypted data log on its SD card. A second Arduino was used by a trusted inspector to decipher the encrypted data log. The demonstration was organized as follows:

1. The Arduino installed inside the CT TEC unit was powered up and the lid was closed;
2. The trusted inspector took notes of the events occurring during the demonstration and the time at which the event was taking place. The tampering attack was simulated by opening the lid of the CT TEC container.
3. At the end of the demonstration, the trusted inspector extracted the SD card and used his own Arduino to decrypt the ciphered messages.
4. The trusted inspector determined that the CT TEC unit was operating correctly upon verifying that his log notebook reflected the same information recovered from the encrypted SD card (similar to the data shown in Figure 3.8).

3.4.4 Final remarks on CT TEC unit

A few notes are here presented to explain what is the expected performance of the CT TEC unit battery. A common zinc-carbon 9 V battery (i.e. model 6F22) used to power the Arduino has a capacity of about 400 mAh. The energy stored in the 9 V battery is:

$$E_{battery} = 400 \text{ [mAh]} \times 9 \text{ [V]} = 3.6 \text{ [Wh]}.$$

A voltage regulator needs to be used to step-down the battery voltage from 9 V to 3.3 V. Modern switching regulators have an efficiency of about 80%-90%. Let's conservatively assume a voltage regulator efficiency of 80%. The remaining energy available to the Arduino is:

$$E_{available} = 3.6 \text{ [Wh]} \times 80\% = 2.88 \text{ [Wh]}.$$

With reference to the operating steps presented in Section 3.5.1, it has to be noted that the initialization step (i.e. step #2) lasts about 18 seconds and consumes 59.4 mW. The energy consumed one-time during the initialization is:

$$E_{initialization} = 59.4 \text{ [mW]} \times (18 / 3600) \text{ [h]} = 0.297 \text{ [mWh]}$$

Let's assume that the wake-up function (as described in step #6 in Section 3.5.1) is implemented to wake up the unit every 5 minutes, which means that the unit will wake up 12 times in one hour. The wake-up function takes about 18 seconds to interrogate the unit and write an encrypted message on the SD card. The amount of energy consumed by the wake-up function is:

$$E_{wake\text{-}up} = 33 \text{ [mW]} \times (18 \times 12 / 3600) \text{ [h]} = 1.98 \text{ [mWh]}.$$

Taking into account the time consumed by the wake-up function, every hour the Arduino operates in idle mode for a remaining time interval of:

$$T_{idle} = 3600 \text{ [s/h]} - 12 \times 18 \text{ [s/h]} = 3384 \text{ [s/h]}$$

The Arduino consumes 3.3 [mW] in idle mode, for this reason the expected amount of energy consumed by the Arduino during the idle mode is:

$$E_{idle} = 3.3 \text{ [mW]} \times (3384/3600) \text{ [h]} = 3.102 \text{ mWh}.$$

The total energy consumption of the unit every hour is:

$$E_{total} = E_{wake\text{-}up} + E_{idle} = 5.082 \text{ [mWh]}$$

The projected battery life is:

$$B_{life} = (E_{available} - E_{initialization})/E_{total} = 566 \text{ [h]}$$ which is about 23.5 days.

By removing the wake-up function, the energy consumed by the wake-up function would totally disappear and the energy consumed during the idle mode would rise to

$$E_{idle,no\ wake\text{-}up} = 3.3 \text{ [mW]} \times 1 \text{ [h]} = 3.3 \text{ [mWh]}.$$

Without implementing the wake-up function, the projected battery life would be:

$$B_{life,\ no\text{-}wake\text{-}up} = (E_{available} - E_{initialization})/ E_{idle,no\ wake\text{-}up} = 872 \text{ [h]}$$ which equals to about 36 days.

3.5 Integrated System

Figure 3.9a displays the fully integrated and operational CT TEC demonstration system with its lid open to expose the interior electronics. Note this shows the system before arming the electronics. The storage area in this container is the volume next to the analog PCB. Figure 9b displays the CT TEC after it has been armed and the container has been opened. Notice the red and green LEDs are lit up in the Figure to denote the violation of the container integrity. Figures 3.10 and 3.11 show more details of the electronics, wiring, and conductive pads.

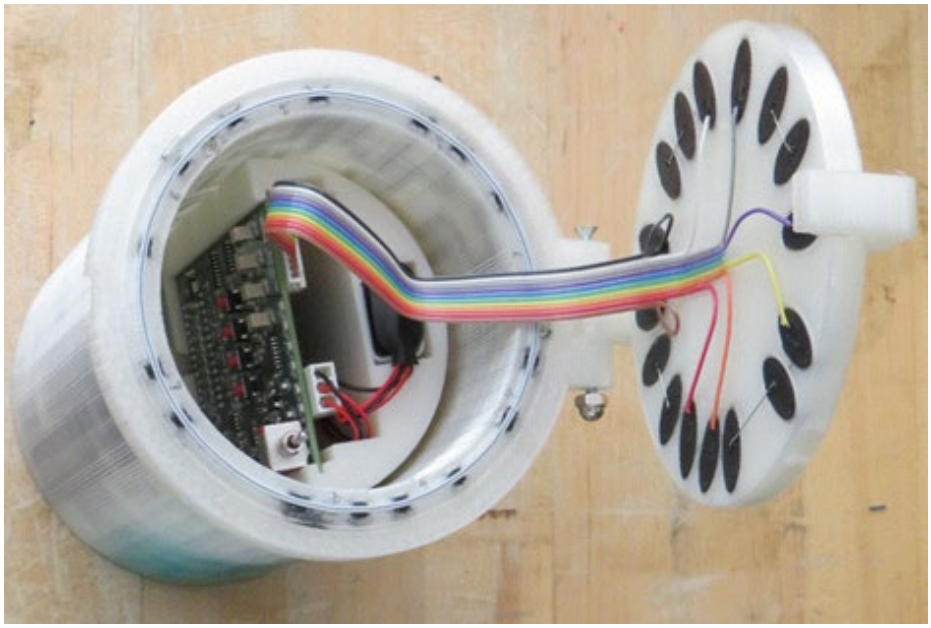

(a)

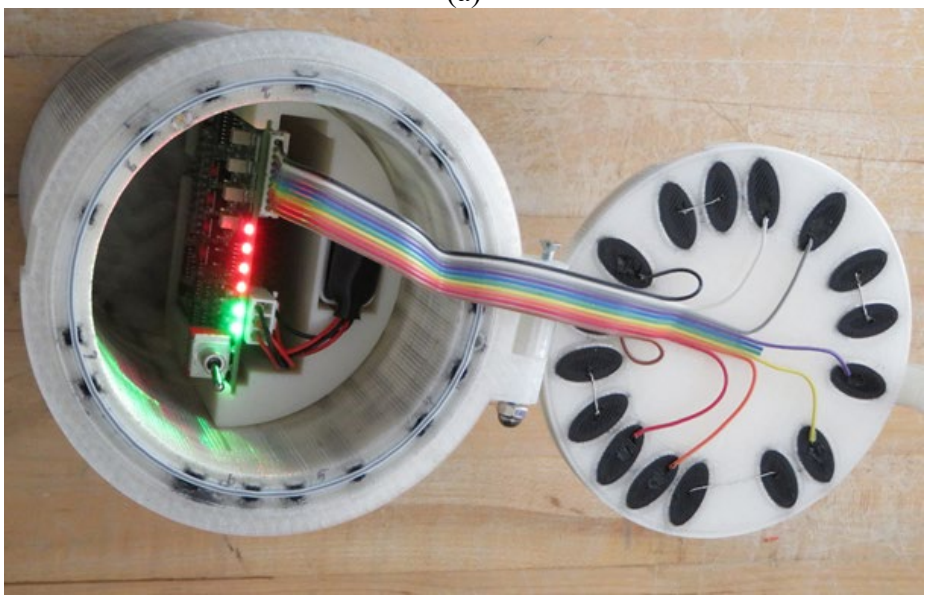

(b)

Figure 3.9. Fully integrated CT TEC demonstration unit with its lid open to expose electronics (a) prior to arming and (b) after arming and then re-opening the container to trip its detector circuitry.

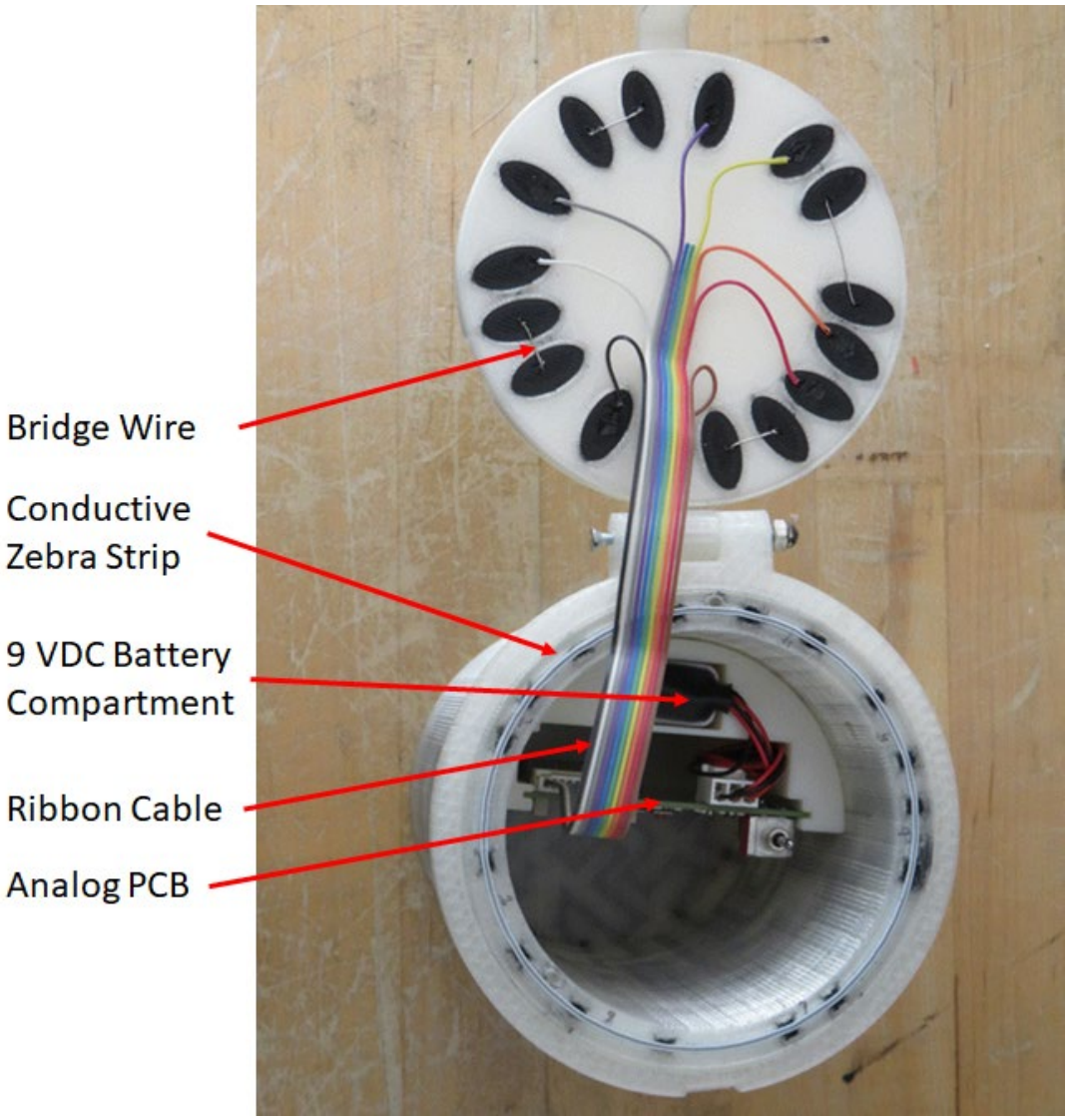

Figure 3.10. CT TEC showing greater detail of the bridge wires on the lid, the ribbon cable from the analog PCB to the lid, and the conductive Zebra strip between the container and lid.

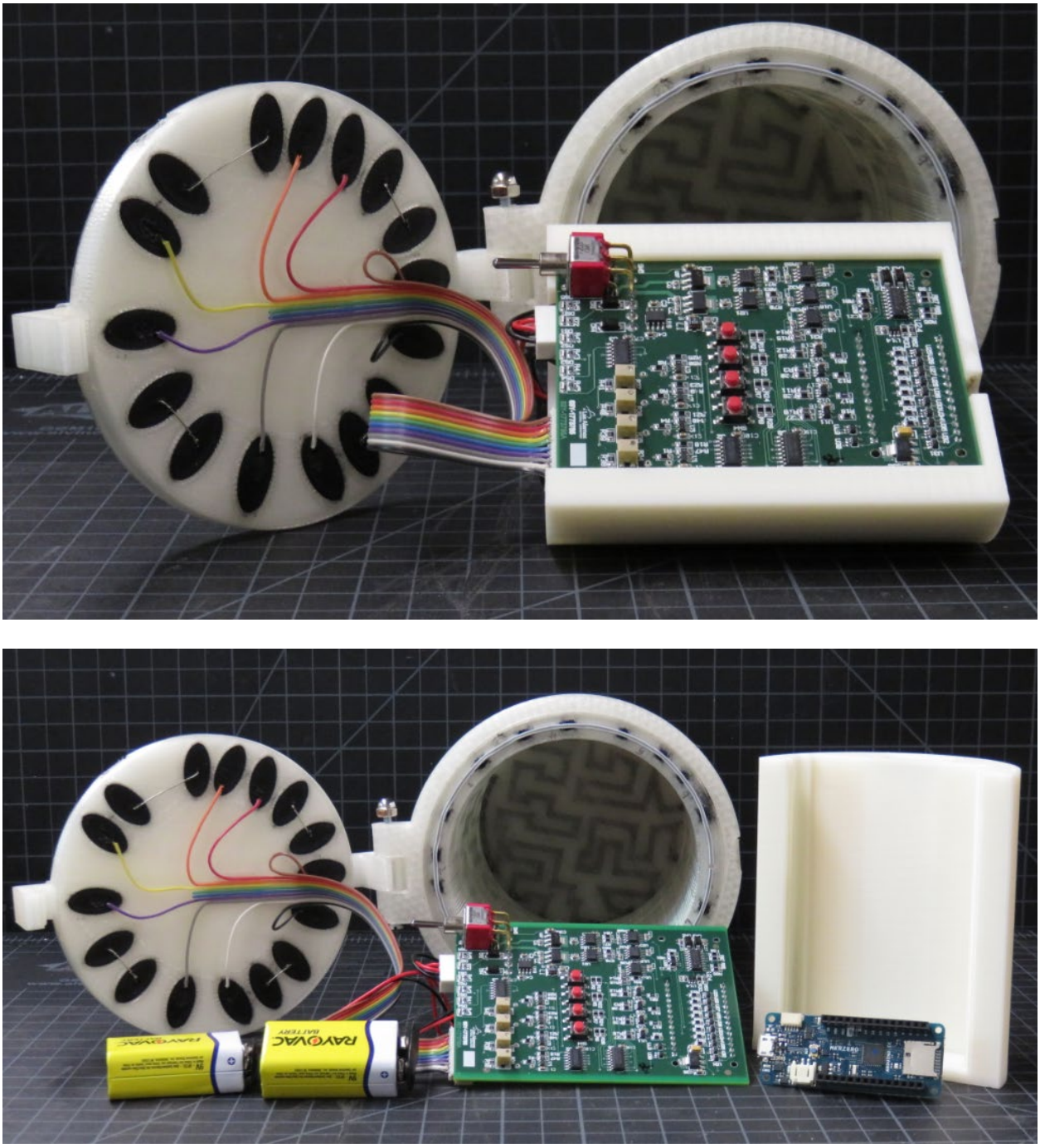

Figure 3.11. Close-up of the CT TEC electronics and their mount removed from the container.

4.0 Fiber Optic (FO) TEC

4.1 Basic Construct of FO-TEC

For many LANL mission-based applications, there has been a strong desire to get away from conductive electronics and transition to optical transmissions. This trend inspired a new design of TEC based on optical traces and connections. This new design involves wrapping optical fiber around a container and *in situ* embedding of this fiber into the walls of the container. This team has prior experience in optical embedded sensing, so this design was a natural progression of previous work. However, many technological challenges were overcome to successfully print a FO-TEC. Bare glass optical fiber, i.e., consisting of only a core and cladding, is extremely fragile and will form micro-cracks with even small amounts of heat or flexion. A thin acrylic sizing layer is commonly coated onto the bare optical fiber to eliminate micro-cracks and losses in light transmission. The sizing-coated fiber is only ~ 200 μm in diameter, making handling and manipulation challenging. An innovative optical fiber laying and coating process was integrated into a restructured commercial Lulzbot Taz printer. The printing process used a commercial fused filament extruder nozzle coupled to a custom optical fiber feeding nozzle to lay optical fiber down and immediately embed it into the polymeric filament (in this case polylactic acid (PLA) was chosen as the base material). Distances between the customized optical fiber feeding nozzle and the filament hot-head nozzle were optimized to fully coat and embed the optical fiber into the filament without over heating the optical fiber and creating micro-cracks. Additionally, a horizontally spinning print surface was also designed with the necessary customized software to print the optical fiber along a horizontally spinning cylinder.

Complications arose during the routing of the optical fiber on the lids of the container because optical transmission was not maintained once the fiber was bent at bend radii less than 16 mm. An innovative routing design was introduced for the optical fiber along the lids with overlapping spirals to fully cover the flat surfaces without over bending the fiber. Lastly in the design, connectorizing the base to the cylinder and to the lid was challenging. As the fiber entered from the exterior surface, it spiraled a full rotation through the wall of the chamber to ensure that the transition between the outer wrappings and the lid edge did not provide an undetectable point of ingress. A channel was designed through the sealing lip in order to accommodate the fiber entering the container from the edge of the lid, and allow opening/closing without damaging the fiber.

4.2 Mechanical Housing

The fiber optic TEC (FO TEC) is made up of two components: a sleeve and a lid for each side of the container. All components were to be wrapped tightly with fiber optic cable. These components were printed and inlayed separately.

The cylindrical sleeve was designed to be the main body of the FO TEC. The sleeve was printed out of ABS material on a Stratasys F370 3D printer, in order to insure accuracy up to 0.02 mm or 0.008 in. The cylindrical sleeve design accounted for several requirements in order to properly deliver a fully wrapped sleeve. The overall height was specified to allow two inches of storage space within the container after final assembly. A 5mm edge at each end of the cylinder was included in order to interface the lid and base with the sleeve. The edge had a diameter of 170

mm, as required by the diameter of the lid and base. Holes were placed at each end of the sleeve, allowing access for the fiber optic to the inside of the sleeve in order to interface with the laser and receiver. These holes were internally swept around the entire circumference to provide fiber optic coverage between the outer wrappings and the lid edge. Lastly, a hole was swept through the bottom face of the sleeve edge to the inside of the sleeve. This provided a slot for the fiber coming from the edge of the lid to prevent crushing the fiber when opening or closing the container. This is shown in Figure 4.1.

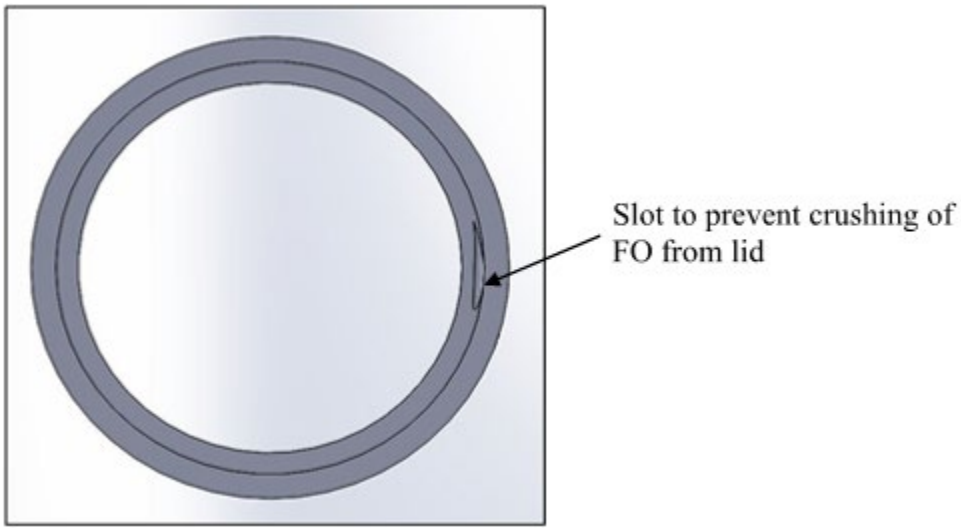

Figure 4.1 Top view of TEC sleeve

In order to wrap the TEC sleeve with FO and fully encase it, modifications were made to a Lulzbot Taz 5 3D printer to print on a horizontal axis cylindrical print bed. Figure 4.2 shows the horizontal rotational stage that was designed and assembled. Side mounting for the horizontal stage was considered but there were concerns regarding the stability of the support as the part that was produced would progressively gain mass. Therefore, the first iteration of the design mounted the horizontal stage vertically to a mounting plate. This plate was designed to mount on top of the z-stage levelling brackets, where the original print bed would normally be placed. This was done in order to level the mount plate in the z-direction, relative to the nozzle of the extruder. The horizontal print stage was designed to rotate on bearings installed on each end of the spin axis to relieve the bending stress on the stepper motor shaft. Radial load ratings for 608-2RS bearings were determined to be beyond sufficient for print sizes exceeding the maximum print volume.

.

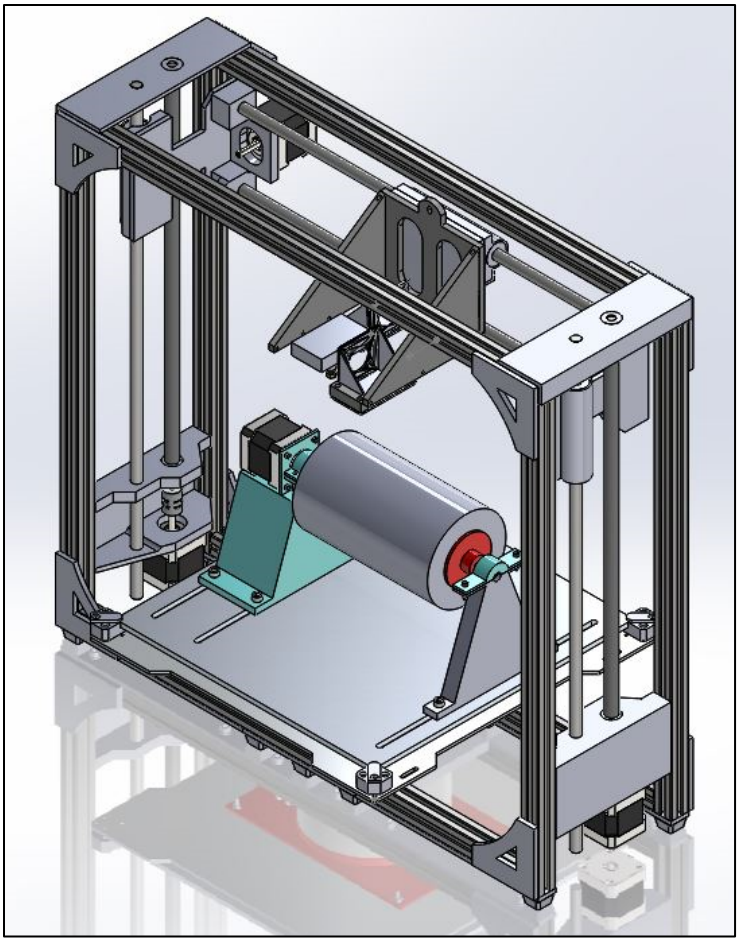

Figure 4.2. CAD model of the new horizontal rotation stage for the Taz 5 3D printer.

Once the design was finalized for the horizontal-axis cylindrical stage, the components were 3D printed and assembled to the Taz 5. The cylindrical print bed was printed on a Stratasys F370 out of ABS material and covered with paint tape to allow reuse of the cylinder. A PVA based glue stick was applied before every print to improve adhesion to the cylindrical print bed. The 3D printed mount plate for the rotational stage had too much deflection once the assembly was mounted. To eliminate deflection, the stage was mounted to a new polycarbonate mount plate, eliminating the issue of deflection. The y-translation stepper motor was replaced with the cylindrical rotation stepper motor. The rotational stepper motor was tested and successfully achieved high angular resolution. G-code was custom written and sent to the printer through the Cura software program to run the rotating stage and control the location of the printer nozzles/extruders. PLA was used for testing and, through several tests and modifications, the printer was successful in printing 26 revolutions (total of 15.6 mm length along cylinder) and additional layers on the cylindrical print bed. The PLA printing process can be seen in Figure 4.3 along with the progression of test print samples. For the initial tests, only one extruder was used in order to test the adhesion of PLA to a cylindrical print bed.

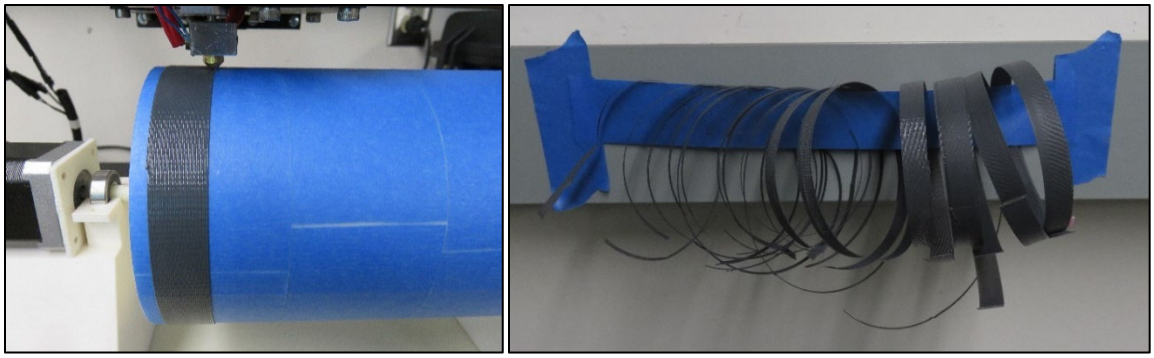

Figure 4.3. Print process for PLA samples. Progression of PLA cylindrical sections.

After successfully printing PLA on the cylindrical print bed, a second print head was adapted to draw 0.2 mm diameter fiber optic cable through a non-heated nozzle, which was subsequently to be wrapped onto the 3D printed cylinder. The newly adapted print head was mounted to align both nozzles in the y-direction. In this new orientation, the two print heads would be capable of laying down fiber optic (FO) on the cylindrical print bed while encasing it with a layer of PLA. The next iteration of G-code was written and started by printing two layers of PLA onto the cylindrical build surface. The next G-code command paused the build to allow sufficient time to tack down the start of the fiber optic at the edge of the rotational stage using tape. Once the fiber optic was successfully attached to the cylinder, the print resumed and wrapped 26 revolutions of FO on top of the first two layers of PLA (15.6 mm of cylinder length). The tension in the fiber optic between the nozzle and the taped down end, held it in place when being wrapped across the entirety of the print. The print job was paused again to tack down the end of the FO (which held the tension between all FO wrappings) and then resumed to print the final two layers of PLA to fully encase it. After several iterations of fine tuning the process, an FOC was successfully encased in 4 layers (2 on each side) of PLA plastic. In each case, the encased fiber optic was tested and successfully demonstrated light transmission.

Once encasing a length of FOC in PLA was successful, the first cylinder was replaced with the final TEC sleeve design. New mounts were printed to allow 13 mm of clearance on the bottom side of the cylindrical print bed. New holes were drilled in the mount plate to account for the difference in mount location due to the change in size between the first print bed and the final TEC sleeve design. The adaptors used to interface the print bed with the bearing and the motor shaft, were modified to fit into the 5 mm edge on either side of the TEC sleeve. Holes were included in the lid adaptors in order to tape down the FO to the inside of the sleeve during the printing process. These adaptors are shown in Figure 4.4. The fully assembled 2nd iteration cylindrical print bed (TEC sleeve print bed) is shown in Figure 4.5. Tests proved successful in printing PLA onto the TEC sleeve after adjusting many parameters, including: the z-offset between the nozzle and the print bed, nozzle feed rate, nozzle temperature and extrusion amount per rotation. The G code was then modified to print a spiral of PLA for the first layer instead of a solid layer in order to provide the fiber optic even distribution around the cylinder. The spacing between each spiral was approximately 0.25 mm wide, allowing enough spacing for the FO to fit between. New G code was written to:

1. Print the spiral layer of PLA.

2. Pause to insert FO into the sleeve through the swept cut hole at the beginning of the spiral and tape down to the inside of the container.
3. Resume the print job and print over the fiber optic with PLA while simultaneously wrapping it.
4. Pause again at the end to insert and attach the other end of fiber optic inside the container.
5. Encase the fiber optic with a solid layer of PLA.

After many tests and adjustments, the print was successful in wrapping fiber along a specified spiral path and simultaneously encasing it with PLA. This is shown in Figure 4.6.

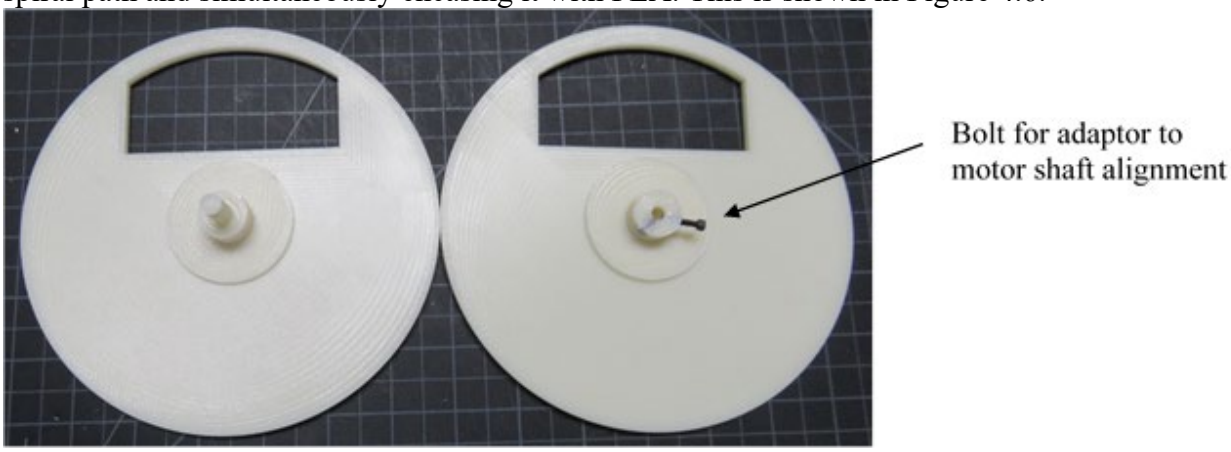

Figure 4.4. Lid adaptors for interfacing bearing and motor shaft to TEC sleeve print bed.

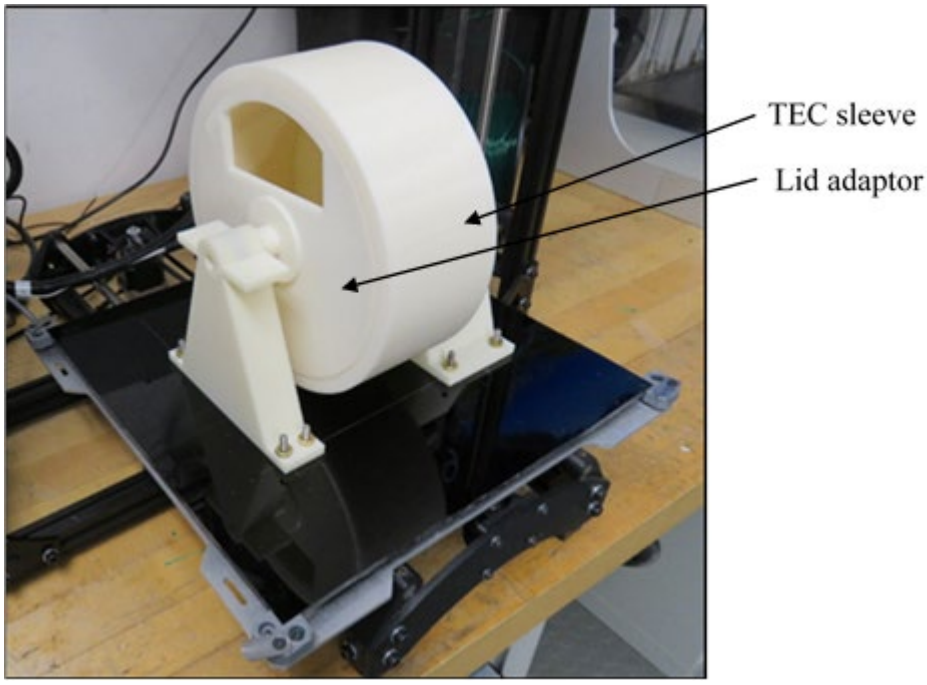

Figure 4.5. Fully assembled, 2nd iteration cylindrical print bed (TEC sleeve).

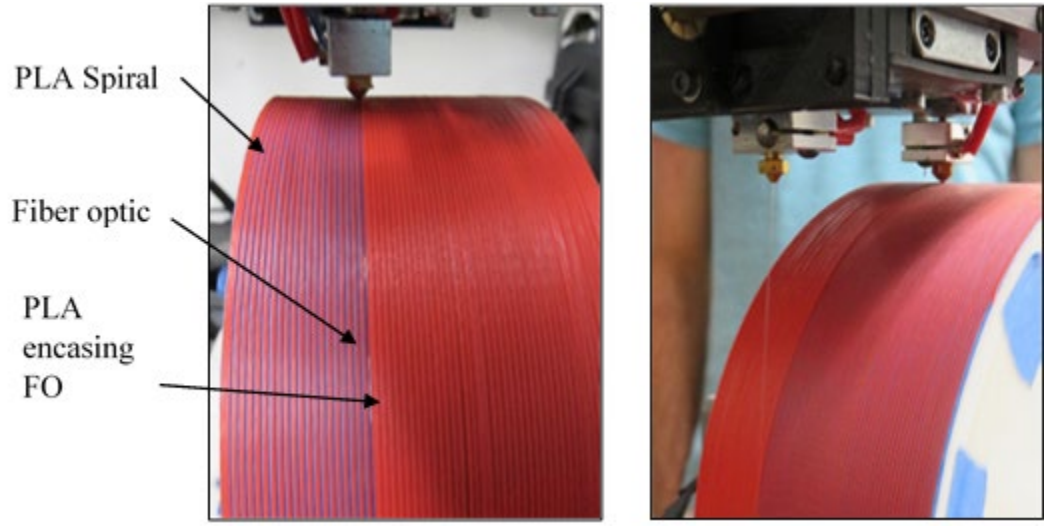

Figure 4.6. Successful PLA spiral and simultaneous PLA/fiber optic embedding.

Throughout the process, many lessons were learned when printing onto the TEC sleeve. The main issue that was encountered was uneven rotation of the TEC sleeve in the z-direction. When rotating the sleeve, it was obvious that some areas of the cylinder were up to 1 mm higher than others. This made adhering to the print bed very difficult, especially when printing the PLA spiral. Several steps were taken to combat the issue of uneven rotation. The first step was to reprint all parts used to mount the cylindrical print bed to the mount plate. This was done on the Stratasys F370 printer to insure accuracy up to 0.2 mm. The same was done for the TEC sleeve and the lid adaptors shown in Figure 4.4. Also shown in Figure 4.4, is a bolt that was adapted to the right side lid adaptor to insure no slippage between the motor shaft and the adaptor. After all of these steps, uneven rotation was greatly reduced. The print was made successful by adjusting the nozzle height offset in the z-direction within a very small margin to allow adhesion at the highest points of the cylinder and even distribution at the lowest points.

The same fiber optic cable being used to wrap the TEC sleeve (Corning SMF-28) was used to lay into the lids but also included a 900 μm jacket around the FO. As previously stated, the minimum bend radii of 16 mm for this fiber optic cable was the main limiting parameter influencing the design of the lid. A square slot sized to be 1.4 mm x 1.4 mm was swept around a spiral throughout the entirety of the lid, leaving ~1 mm of wall thickness for the OD of the lid and a 15 mm radius at the center of the lid. Since the FO can only be wrapped to a 15 mm radius, the center of the lid had a 30 mm diameter without FO wrapping, leaving that area exposed. In order to account for the exposure in the first lid, a second lid was modeled offset from the center of the first lid and would also be wrapped with FO down to a 15 mm radius. For the outer wrappings of FO in the second lid to cover the exposed 30 mm diameter at the center of the first lid, the outer diameter of the second lid feature would need to be 90 mm, making the first lid feature OD 170 mm. The sizing and coverage of the lid are shown in Figure 4.7. The first and second lids were made into one piece and the fiber optic cable was made continuous throughout the entirety of the lid. This was done to improve the efficiency of the design and avoid the need to splice the FO connection between each of the lid features. A slot at the exit of the first FO

spiral, 2 mm from the OD of the first lid feature, was included to avoid crushing the fiber when closing the lid while maintaining maximum coverage.

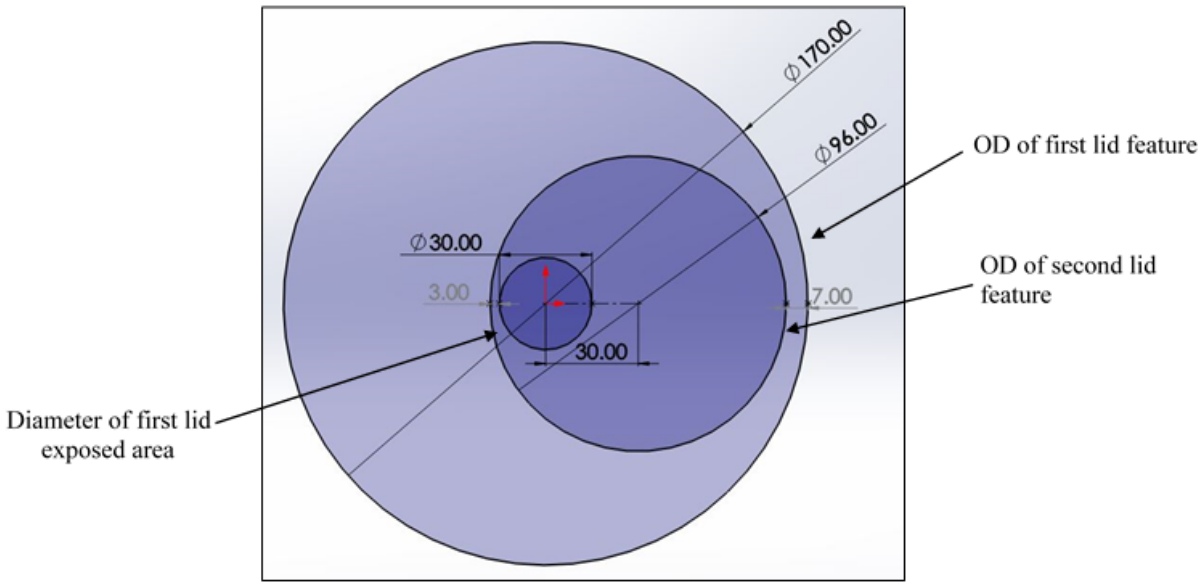

Figure 4.7. Top and bottom lid sizing diagram.

The lid and base were printed out of ABS on an Ultimaker S5 3D printer. To inlay the FO into the lid, the print was paused using the "pause print at layer number" feature in Ultimaker Cura 4.2. The FO was then laid into the first spiral in the lid using a thin layer of PVA based glue stick. A straight slot was made extending from the end of the spiral at the center of the lid to the OD of the lid to hold the place of the remainder of the FO for the second spiral. The FO spool was placed outside of the 3D printer chamber and the print was resumed covering the entirety of the first FO spiral with the next layer. The print was paused again after completing the second set of spirals. The slot between the first and second set of spirals, allowed continuity of the FO throughout the entirety of the lid. The same process was followed to inlay the FO into the second set of spirals as the first. Another straight slot extending from the center of the second set of spirals to the OD of the second lid feature, allowed for the placement of the remainder of the fiber. This slot was included to prevent the 3D printer nozzle from colliding with the FO while finishing the print. After both sets of FO spirals were laid into the lid, the print resumed and finished, leaving a lid that had full FO coverage and encasement. This design was printed twice and used for the lid and base of the Tamper Evident Container. This entire process is shown in Figures 4.8, 4.9, and the final lid in 4.10.

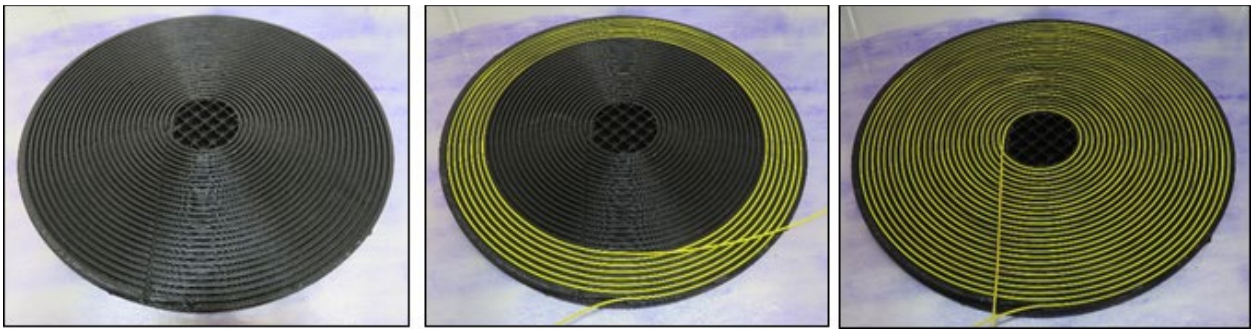

Figure 4.8. TEC lid print, Spiral #1, FO inlay process.

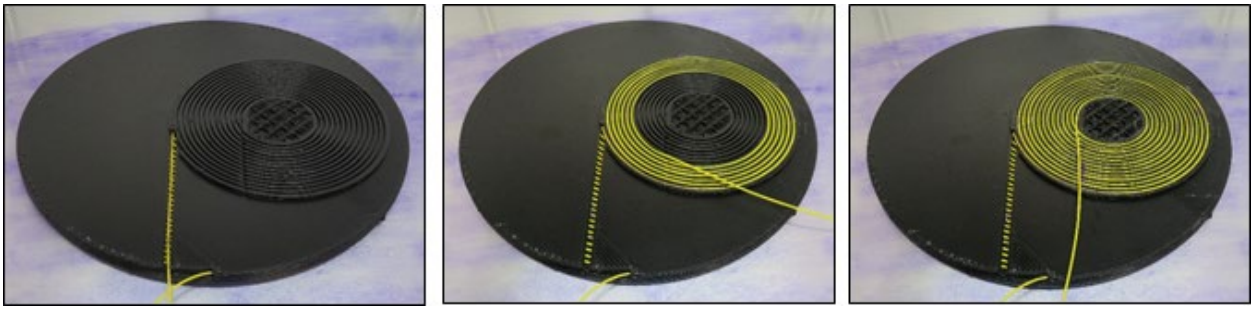

Figure 4.9. TEC lid print, Spiral #2, FO inlay process.

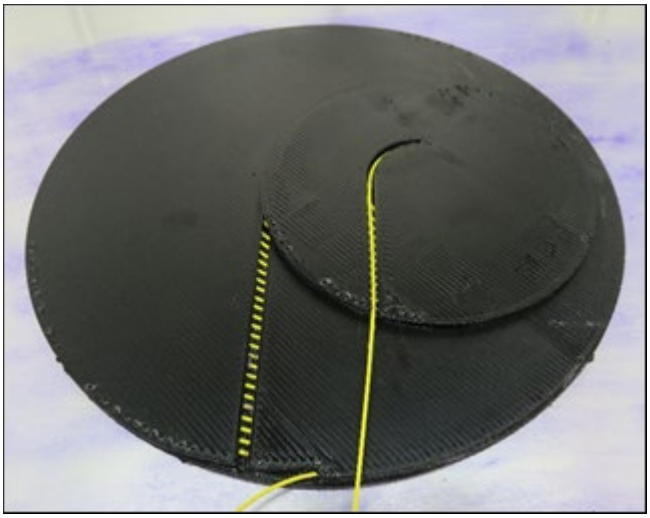

Figure 4.10. Completed TEC lid print with full FO coverage.

Once the lid, base, and sleeve were printed and wrapped with fiber optic cable, the process began to connect and interface between each of the sets of FO. The end of fiber optic coming from the middle of the lid was spliced to the end coming from the wrapping of the sleeve on each side. Before splicing the sleeve end, a 900 µm jacket was slipped around the outside of the 200 µm acrylate coated FO to further protect it. The Fujikura 70S splicer (Figure 4.11) and the procedure outlined in its instruction manual were used to splice each of these ends. A heat shrink splice protection sleeve was used to protect the spliced area between the two ends. The other two ends

of FO coming from each lid were connectorized to interface with the laser and the receiver. The end interfacing with the laser is an SMA connector, while the side interfacing with the receiver is an FC/PC connector. The process outlined in the Thorlabs Guide to Connectorization and Polishing of Optical Fibers (FN96-A) was followed to connectorize and polish the SMA and FC ends.

(a)

(b)

Figure 4.11. (a) Fujikura 70S+ Fusion Splicer powered on at main menu with fiber mounted into splicing holders and (b) Screen captures from the Fujikura 70S+ during the fiber splicing process. Left: Fiber pre-splice during the alignment phase. Right: Fiber post-splice with estimation of transmissivity loss of new fiber.

After splicing and connectorizing each of the FO ends of the TEC, the container was assembled starting with the base, which was super glued to the bottom of the TEC sleeve. A false bottom and standoffs were modeled and 3D printed to allow sufficient space for the electronic components while maintaining the storage space of 2 in above the false bottom. Magnets were placed into the bottom face of the false bottom and the top of the standoffs in order to establish a secure connection. A hinge for the top lid was designed to have an offset above the container to avoid crushing the fiber optic when lifting the lid. An arm and knob were also printed to attach to the top lid. Finally, a hinge stopper was designed to stop the lid from extending too far and breaking the fiber optic. A CAD model of the fully assembled Fiber Optic Tamper Evident Container is shown in Figure 4.12.

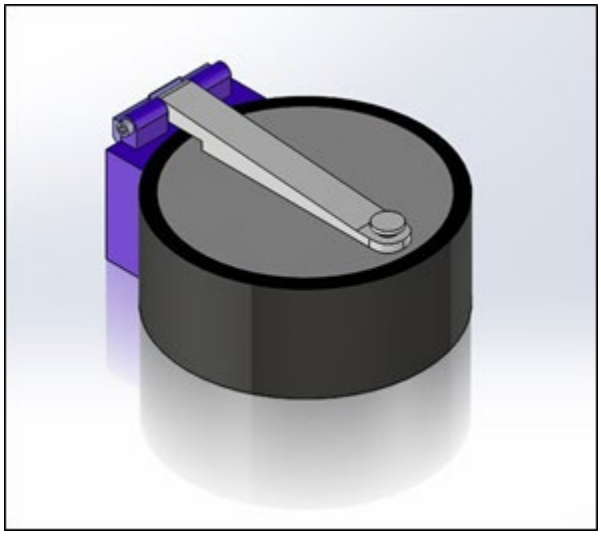

Figure 4.12. Fully assembled Fiber Optic Tamper Evident Container.

4.3 Analog Electronics

A concept was developed for the Fiber Optic (FO) electronics using 4 fixed free running bistable mlutivibrators (oscillators). The concept consisted of using 4 discrete 7555 timers, set up as free running oscillators, that could be reset or enabled from the CPU. Each timer circuit has a fix frequency that was not a multiple of any other frequency used. Refer to schematic 63Y-1773758_2A, Figure 4.13.

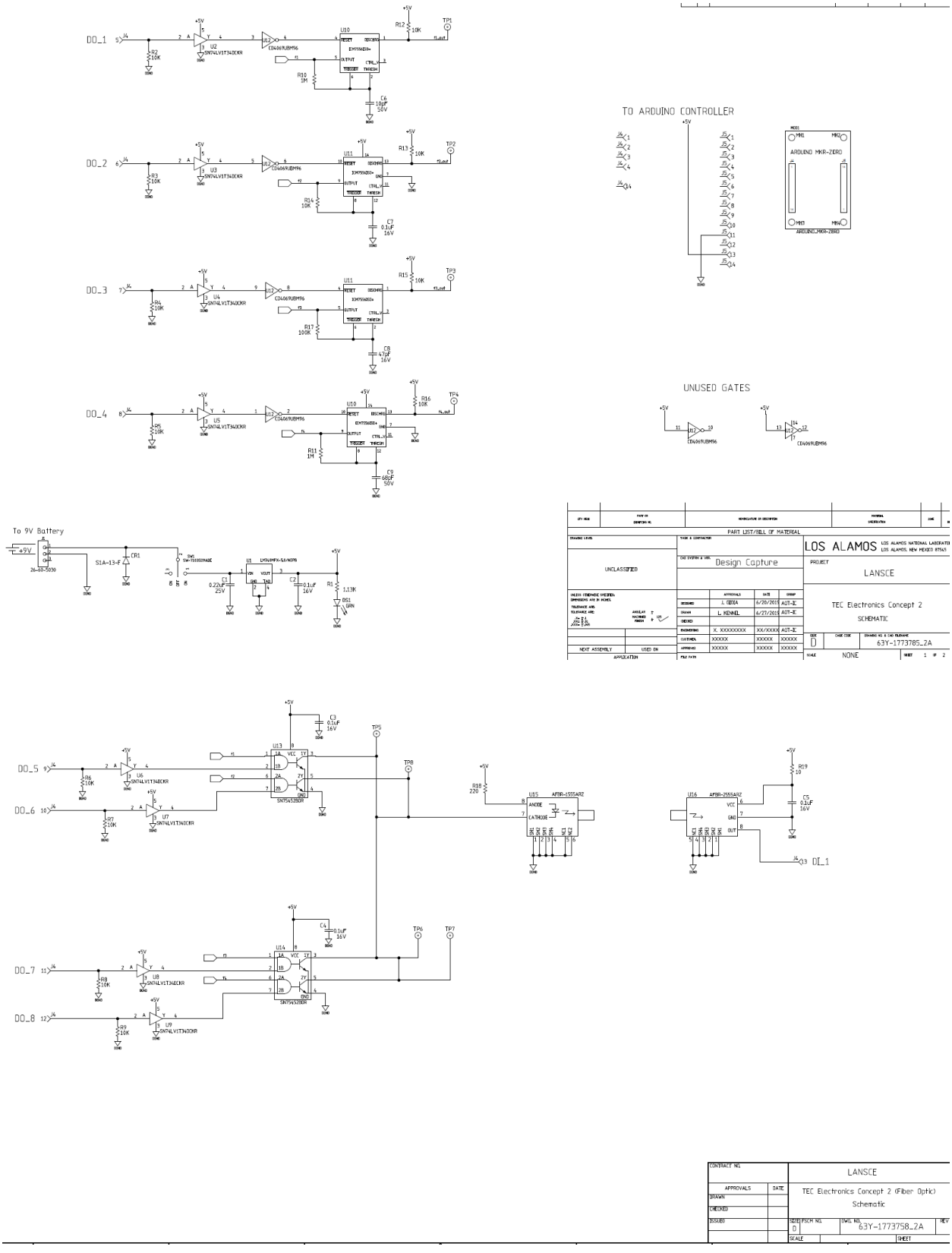

Figure 4.13. Analog circuit schematic of a fiber optic light source and detection system.

A single 9V battery was employed driving a 5V regulator to power the circuit electronics. The 4 discrete frequency outputs of the timers were sent to two AND gate dual Integrated Circuits (IC) with "Open" collector transistor outputs which can be tied together. By enabling one of the AND inputs and feeding the other with one of the frequencies we develop a frequency to drive the FO transmitter diode. A receiving FO diode, via FO cabling, then translates that frequency to the CPU digital input. Using a combination of frequencies and enabled gates, we can generate a unique frequency signature that can only be interpolated by the CPU.

The CPU could also be programmed to output 4 different frequencies for an endless combination of frequency spectrum. This discrete approach with fixed frequencies was chosen as a quick means to show Proof-of-Concept.

This technique was not implemented as the fiber produced by the 3D printing methodology was not compatible with the FO transmitter/Receiver pair. Time only allowed us to implement the present demo. To resolve this incompatibility, the team employed a Thor Labs photo detector that was compatible with the existing laser and output an analog signal that Arduino board could track.

4.4 Digital Electronics & Software

The Arduino installed in the FO TEC unit is programmed similarly to the one used in the CT TEC unit (see Section 3.4.1). The major differences between the FO TEC Arduino and the CT TEC Arduino are related to the fact that the FO TEC unit is equipped with analog circuitry different from that used in the CT TEC unit. These differences can be better understood by comparing Figure 3.7 to Figure 4.14.

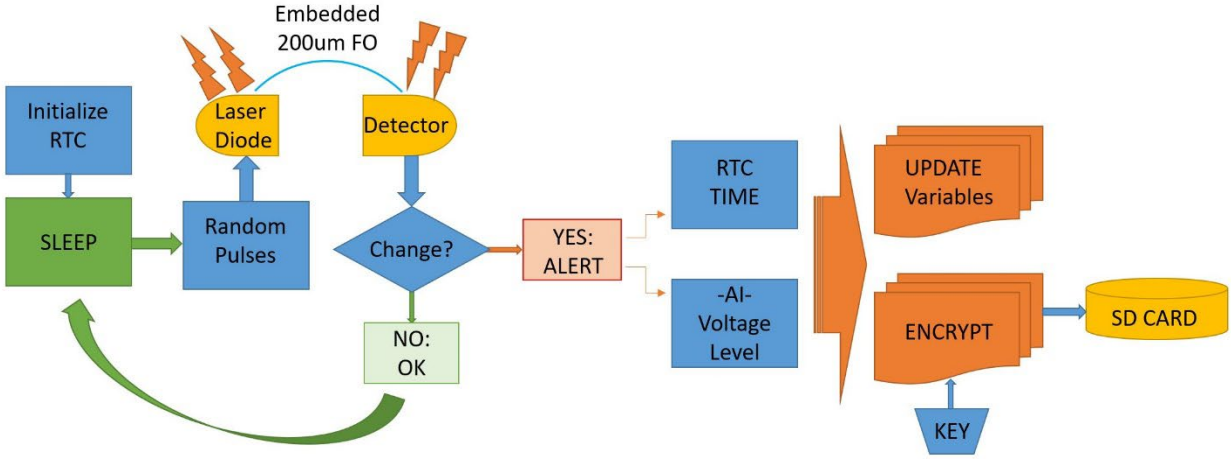

Figure 4.14. CT TEC Arduino's operation flow chart.

FO TEC Arduino's operation and encryption details are provided in Sections 4.4.1 and 4.4.2, respectively. Further, Section 4.4.3 shows how Arduino's operation and encryption are used in the FO TEC demonstration.

4.4.1 FO TEC Operation

Although the Arduino functions nearly identically to the CT TEC's, there are some distinctions. RTC, SD card, and encryption initialization still occur after a 30 second opportunity to close the lid. There is no other logic board to integrate with, but the Arduino does integrate with a laser diode and photodiode.

Detection of attempted ingress is accomplished by pulsing laser light through the embedded fibers. These pulses happen at random intervals within each successive second, as determined by the Arduino. Light is received by a reverse-biased photodiode, allowing current to flow across a voltage divider. Reading ADC input from this divider, the Arduino can determine if there has been transmission loss due to bending or breaking of the fiber. An encrypted data log will be created in the event of transmission loss or increase, or a constant transmission signal with no return to ground (attempted bypass). Encrypted data will be written to the card regularly, verifying system function through time, for diagnostic purposes.

In the event of total transmission loss, the Arduino will cease pulsing the laser to ensure the safety of handling personnel. It would be assumed that the fiber has been broken at this point. As an engineered control for technician safety, the lid engages two switches connected in series along the laser diode's power input wire.

4.4.2 FO TEC Encryption

The FO TEC encryption algorithm is the exact same used in the CT TEC unit.

4.4.3 FO TEC Demonstration -

To demonstrate the FO TEC capabilities, an inspector will need the FO TEC and a decryption Arduino. The steps are as follows:

1. Open the lid completely and bypass lid safety switches with tape.
2. Remove the false bottom and set aside. The circuit and excess fiber will now be exposed.
3. Lift a length of the excess fiber out of the bottom and hang outside container.
4. Turn on the circuitry and wait 30 seconds.
5. After an additional 10 seconds, simulate an attack by bending the length of excess fiber to a radius of approximately 15mm. Release, repeat, release.
6. To simulate transmission failure: remove tape from one of the lid safety switches.
7. Power down circuitry and remove SD card.
8. Install SD card into secondary Arduino to observe decrypted data.

First, the data should show the voltage variances that occurred during step #5. Then, the data should declare the total transmission loss event.

4.4.4 FO TEC Power Consumption

Assuming the same battery, initialization current, and idle current, the primary difference in power consumption for the FO TEC is the need to drive a 28mA laser. Also, the photodiode uses

an independent A23 (12 volt) battery to provide a voltage bias, and current across the voltage divider.

Power consumption of the laser running at 28mA and 1.9V forward voltage, directly from battery (no regulator inefficiency):

$$E_{laser} = 28\ [mA] \times 1.9\ [V] = 53.2\ [mW]$$

Power burned by current-limiting resistor for laser diode, directly from battery (no regulator inefficiency):

$$E_{resistor} = 28\ [mA] \times 7.1\ [V] = 198.8\ [mW]$$

Total unregulated power to run the laser each pulse:

$$E_{pulse} = E_{laser} + E_{resistor} = 53.2\ [mW] + 198.8\ [mW] + 8.58\ [mW] = 260.58\ [mW]$$

Power used by Arduino during each wakeup and output trigger, compensated for power regulator efficiency of 80%, plus the energy to pulse the laser:

$$E_{wakeup} = (17\ [mA] \times 3.3\ [V] \times 1.25) + 260.58\ [mW] = 330.705\ [mW]$$

Regulator compensated power consumption during wakeup, trigger, and system check write function, plus the energy to pulse the laser:

$$E_{write} = (24\ [mA] \times 3.3\ [V] \times 1.25) + 260.58\ [mW] = 359.58\ [mW]$$

Regulator compensated power consumption for idle:

$$E_{idle} = 3.3\ [mW] \times 1.25 = 4.125\ [mW]$$

Time per hour taken by idle, wakeup, and write (every 5 minutes) operations:

$$T_{write} = (0.001\ [s] \times 12) / h = 0.012\ [s/h]$$
$$T_{wakeup} = (0.001\ [s] \times (3600 - 12)) / h = 3.588\ [s/h]$$
$$T_{idle} = (3600[s] - 0.012[s] - 3.588\ [s]) / h = 3596.4\ [s/h]$$

Energy consumed per hour, by all operations:

$$E_{total} = (E_{write} \times T_{write}) + (E_{wakeup} \times T_{wakeup}) + (E_{idle} \times T_{idle}) =$$
$$(359.58\ [mW] \times (0.012/3600)\ [h]) +$$
$$(330.705\ [mW] \times (3.588 / 3600)\ [h]) +$$
$$(4.125\ [mW] \times (3596.4 / 3600)\ [h]) = 4.451\ [mWh]$$

The projected battery life is:

$$B_{life} = (E_{battery} - E_{initialization})/E_{total} = 808\ [h]$$ which is around 33 days.

The photodiode runs on a separate A23 (12 volt) battery, that Thor Labs approximates will last 40 hours at a constant 1mA load. The FO TEC is drawing a 4mA load when pulsing. Since each pulse lasts 1ms, the battery should last:

$$B_{load} = 40\ [mAh] / 4\ [mA] = 10\ [h]$$
$$B_{total} = B_{load} / (T_{wakeup} + T_{write}) = 10\ [h] / (3.6\ [s] / 3600\ [s]) = 10{,}000\ [h]$$ (about 416 days)

Unfortunately, there is an unknown dark current through the photodiode. It is highly unpredictable and variable, but typically is in the micro-amp range. Nevertheless, this battery should outlast the 9V providing power to the Arduino.

4.5 Integrated System

Figure 4.15 displays the fully integrated and operational FOTEC demonstration system with its lid open to expose the fiber optic, light source, and interior electronics. Notice how the fiber optic is one continuous cable. This FOC connects to the laser via an SMA connector at one end, passes through the container to the outer covered layer of the cylinder, passes through to the lower lid, then comes back up through the container to the upper lid, before returning to attach via another FC connector the photo diode detector. The overall length of the fiber used in this demonstration unit was more than 50m. The electronics are housed within a protective enclosure with a lid so that a payload can be placed within the container without damaging the fiber or electronics (see Figure 4.16).

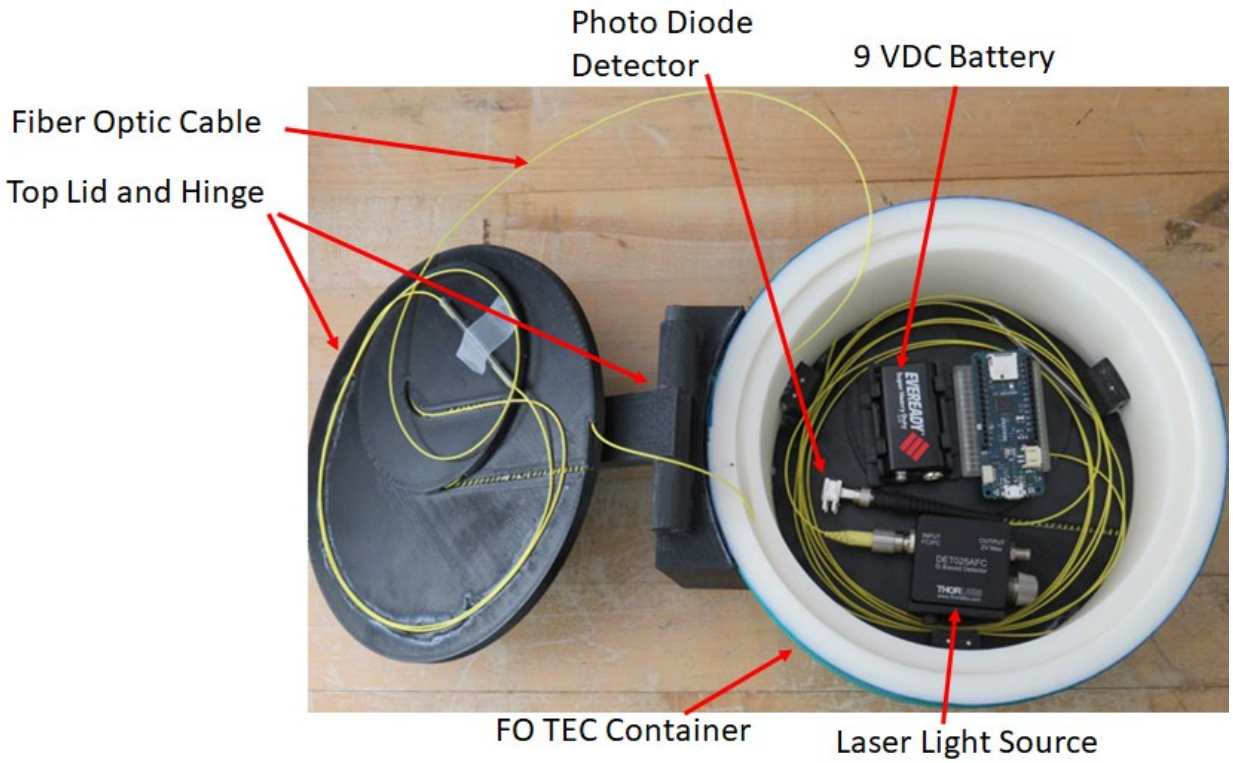

(a)

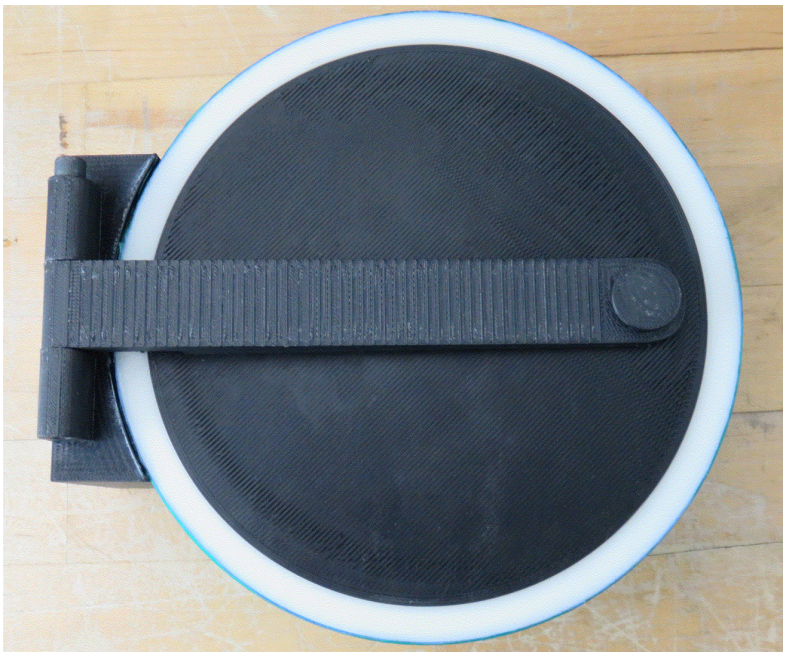

(b)

Figure 4.15. Fully integrated FOC TEC demonstration unit (a) with its lid open to show fiber optic cable, laser light source, and electronics and (b) with lid closed.

Figure 4.16. Fully integrated FOC TEC demonstration unit with cover over electronics bay and with a payload (iPhone) in the storage area.

5.0 Vibration Sensing TEC

5.1 Basic Construct of a Vibration Sensing TEC and Test Configuration

The basic characteristics of mechanical vibration propagation in a mechanical structure, such as amplitude attenuation and phase shifting, are dependent on both the material properties and geometry of the structure. Consequently, if a vibration generator and transducer are used to propagate and measure a mechanical disturbance through a container, they should be capable of serving as tamper evident sensor through detection of geometrical manipulation of the container structure, as shown in Figure 5.1.

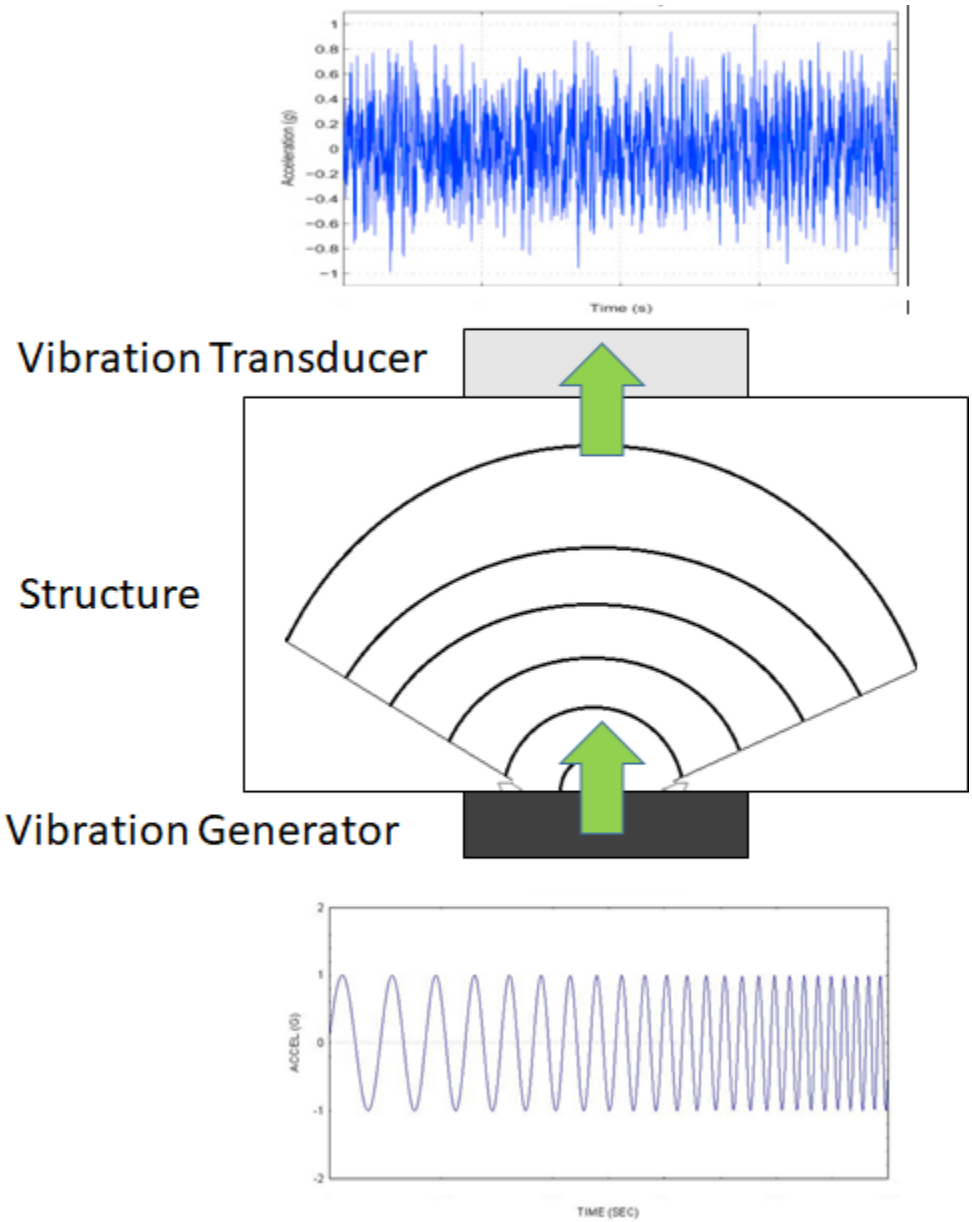

Figure 5.1. Basic detection scheme for a vibration sensing TEC.

To test the sensitivity of this sensing concept, a number of plastic ABS test coupons, 3" square, 0.5" thick, with different infill patterns were 3D printed. As shown in Figure 5.2a, different infill patterns including solid, hatch, and honey comb, the latter with low and high density versions, were made for a horizontal configuration where the part was 3D printed with the 3" by 3" surface laying flat on the 3D printer build plate. These same infill patterns were produced in vertically oriented parts, shown in Figure 5.2b. Each coupon, because of its unique geometry, should have a different mechanical output signal for the same input.

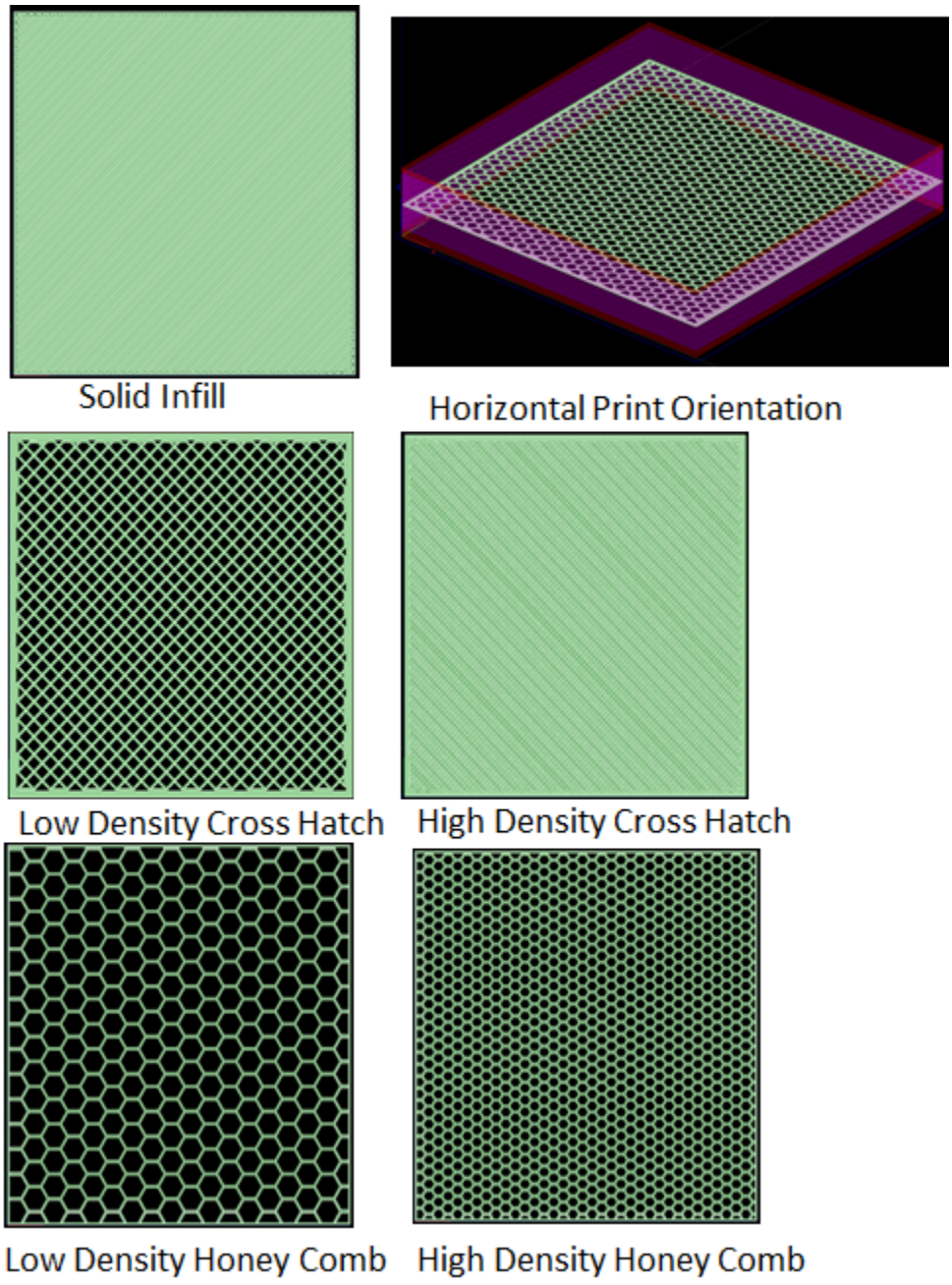

Figure 5.2a. Example test coupon geometry and various in-fill patterns for the horizontally 3D printed parts.

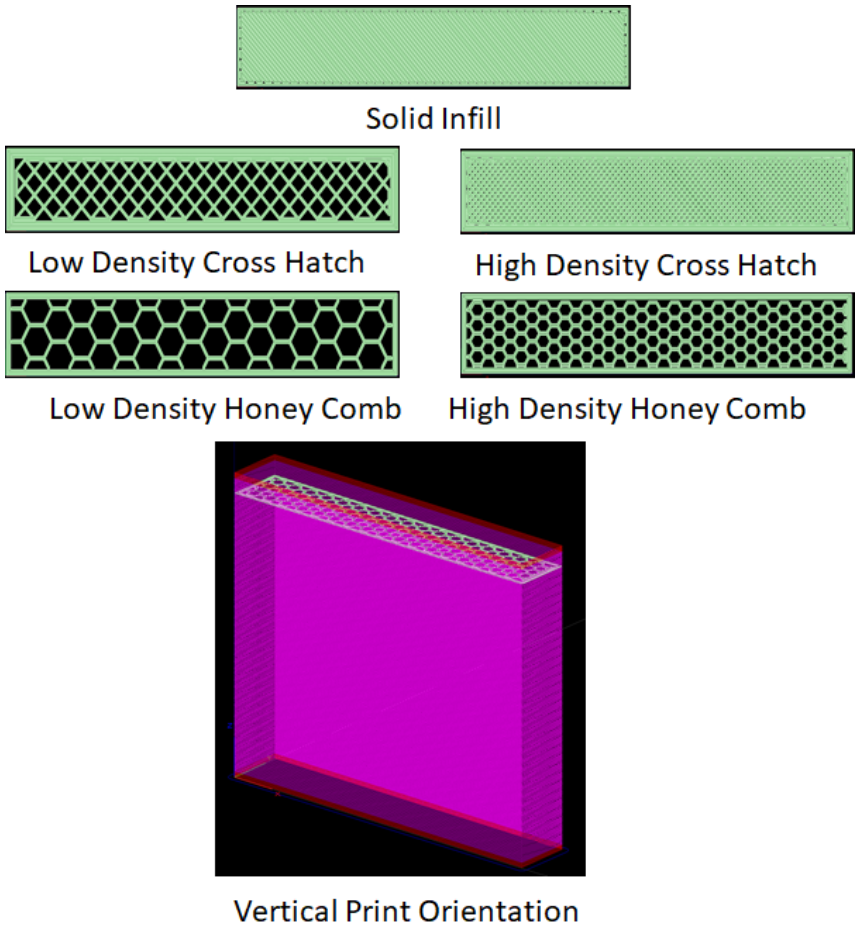

Figure 5.2b. Example test coupon geometry and various in-fill patterns for the vertically 3D printed parts.

In this study a pulsed electrical signal was transmitted through piezo-electric transducers (PZTs) on 3D-printed ABS plastic plates and compared the output to see if plates of different infill patterns could be distinguished. The setup is shown in Figure 5.3. The function generator is an Agilent 33210A model, manually triggered for a linear frequency sweep between 100 Hz and 20kHz in 0.1 s. The oscilloscope is a Tektronix TDS 3034C model, capturing 10,000 points in 0.2 seconds for a Nyquist frequency of 25 kHz.

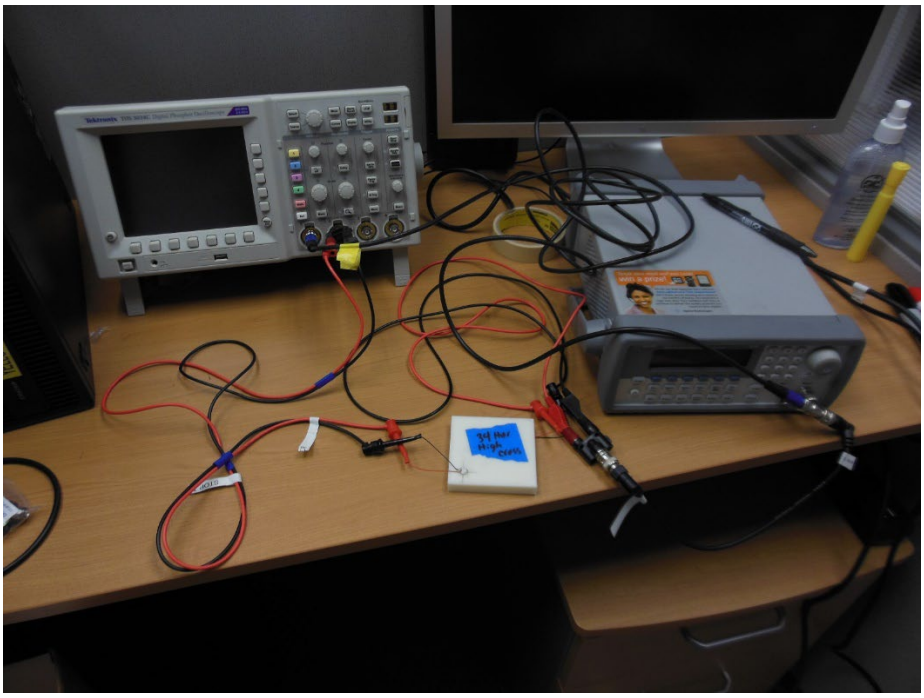

Figure 5.3. Setup for measuring vibration transmission. The sample (white) is in the center, the oscilloscope is on the left and the function generator is on the right.

5.2 Sensing Scheme Assessment

Measurements

Data were taken in 4 sets. In all sets, five measurements were taken for each coupon, which was labeled by marker on a piece of tape. The names of the csv files are shown in Table 5.1. The files contain time (column 1), input (column 2, for some tests) and output (column 3) data. Each set is described following the table. The sample descriptions correspond to the illustrations in Figure 5.2.

Table 5.1. Data file names for all measurements. Figures 5.2a and 5.2b show the infill pattern corresponding to names in the description ("hex" here corresponds to "honey comb" in the figure). The numbers in the description identify each individual coupon. The "correlation index" column gives the numbers used later in the correlation matrices, with sets 1 and 4 treated separately from sets 2 and 3.

Set	File names	Correlation index	Description
1	TEK00001-TEK00005	1-5	Vertical solid 1
	6-10	6-10	Vertical solid 3
	11-15	11-15	Vertical solid 4
	16-20	16-20	Horizontal solid 26
	21-25	21-25	Vertical low cross 14 (black)
	25-30	25-30	Vertical low cross 14 (white)
	31-35	31-35	Vertical low cross 11 (top)
	36-40	36-40	Vertical low cross 11 (bottom)
	41-45	41-45	Horizontal low cross 30
2	TEK00046- TEK00050	1-5	Vertical low hex 9
	51-55	6-10	Vertical low hex 6
	56-60	11-15	Vertical low hex 8
	61-65	16-20	Horizontal low hex 28
	66-70	21-25	Horizontal high hex 32
	71-75	25-30	Vertical high hex 16
	76-80	31-35	Vertical high hex 18
	81-85	36-40	Vertical high hex 19
	86-90	41-45	Vertical high cross 23
	91-95	46-50	Vertical high cross 21
	96-100	51-55	Vertical high cross 24
	101-105	56-60	Horizontal high cross 34
3	TEK00106- TEK00110	61-65	Vertical low hex 6
	111-115	66-70	Vertical high hex 16
	116-120	71-75	Vertical high cross 23
	121-125	76-80	Horizontal high cross 34
4	TEK00126- TEK00130	46-50	Vertical solid 1
	131-135	51-55	Vertical solid 3
	136-140	56-60	Vertical solid 4
	141-145	61-65	Vertical low cross 14 (black)
	146-150	66-70	Vertical low cross 14 (white)
	151-155	71-75	Vertical low cross 11 (top)
	156-160	76-80	Vertical low cross 11 (bottom)
	161-165	81-85	Horizontal low cross 30

Set 1 used nine samples, one of which, "vertical solid 4," is shown in Figure 5.4. These samples have a large and a small PZT; the function generator was attached to the small PZT and the oscilloscope to the large PZT. Four sets of measurements within the set were different from the other five. The label "vertical low cross 14" was applied to two different coupons, which were distinguished only by one being black and the other, white (all other coupons in the experiment

were white). The “vertical low cross 11” coupon had a pair of PZTs on both 3” square faces, so one face was label “top” and the other “bottom” with pen on a piece of tape for identification. Also, the “horizontal low cross 30” and “horizontal solid 26” coupons have two small PZTs; we used only the one nearest to the large PZT for these measurements.

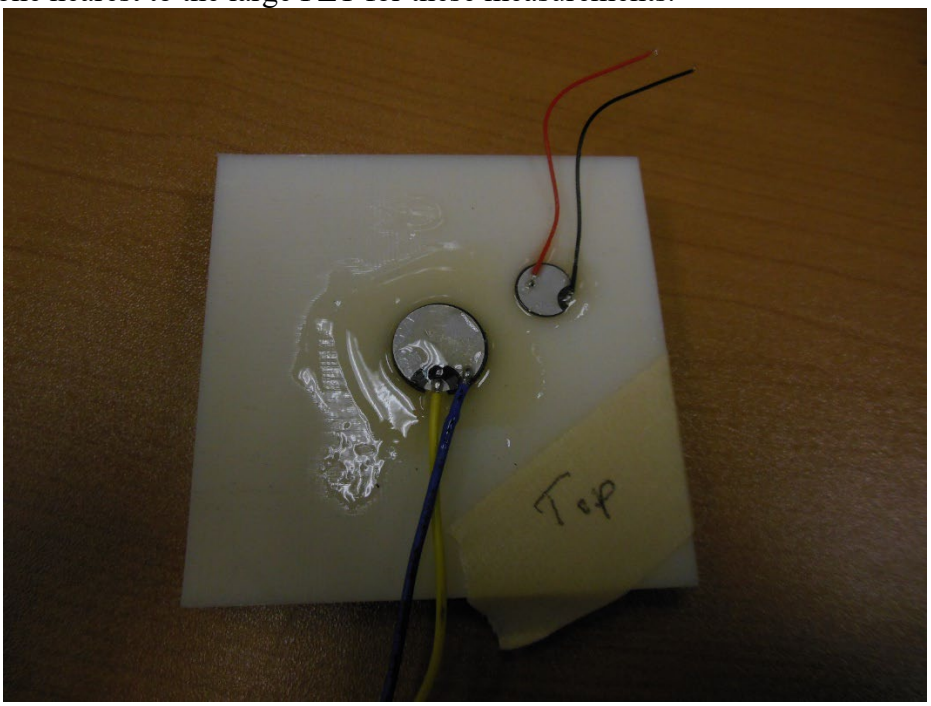

Figure 5.4. The “vertical solid 4” sample from set 1. The function generator was attached to the smaller transponder and the oscilloscope to the larger sensor. Note that the label “top” is superfluous for this coupon since only “vertical low cross 11” had sensors on the “bottom.”

Set 2 used twelve samples, one of which, “vertical high cross 23,” is shown in Figure 5.5. Both PZTs are the small size from set 1 and were placed 0.5” from opposite corners, on opposite sides of the thickness. All coupons were made according to this standard without the deviations of set 1.

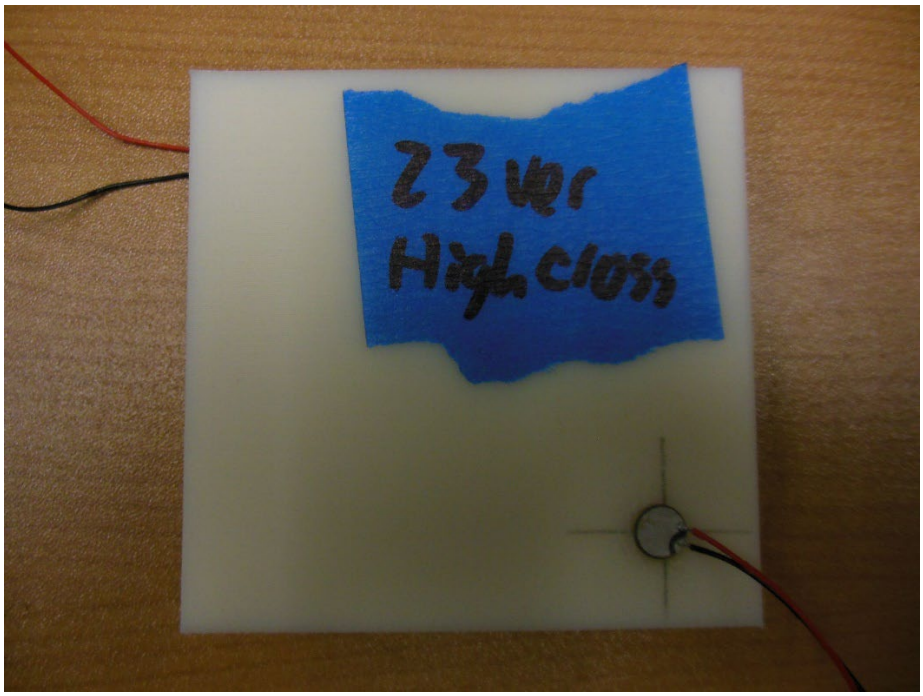

Figure 5.5. The vertical high cross 23 sample from set 2.

Set 3 is an extension of set 2. Four samples from set 2 were drilled with a 0.25” hole in center of the face (see Figure 5.6). Otherwise, they are the same as in set 2. The goal was to see if the PZT signals detect damage by giving a different output than the same coupons measured without the hole.

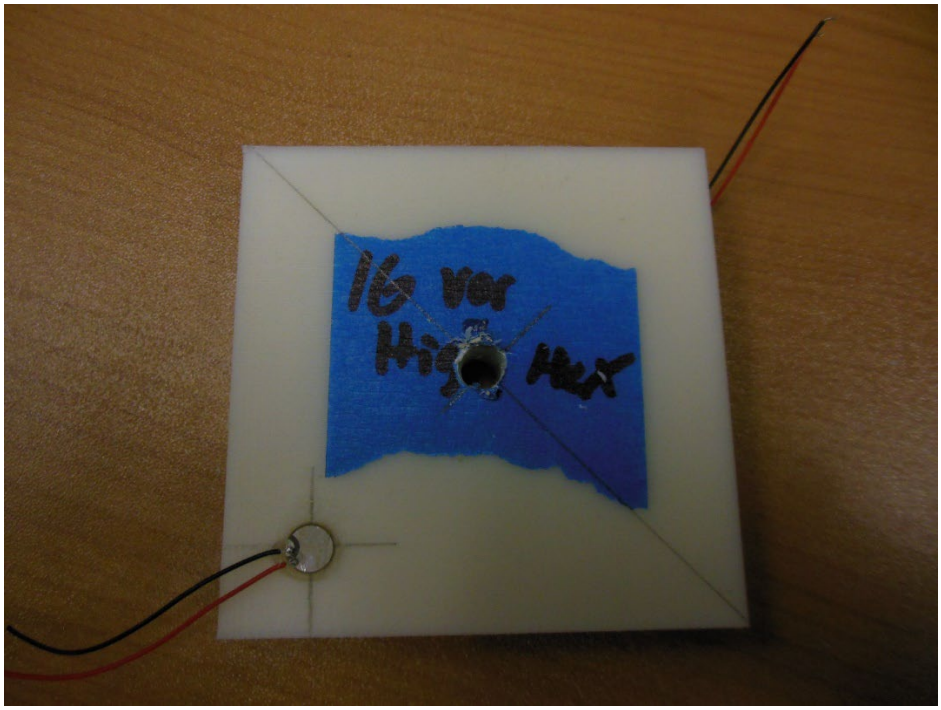

Figure 5.6. The vertical high hex 16 sample from the set 3.

Set 4 is an extension of set 1. We wanted to apply the procedure of set 3 to the coupons in set 1. Due to the lack of uniformity, however, we drilled a 0.25" hole between the PZTs when possible, or next to the PZTs when the PZTs were too close to each other. This was applied to 7 of the 8 coupons used for set 1 (see Figure 5.7). Only for "vertical solid 3" was it possible to drill directly between the PZTs; for all other coupons, the PZTs and the hole locations formed a triangle.

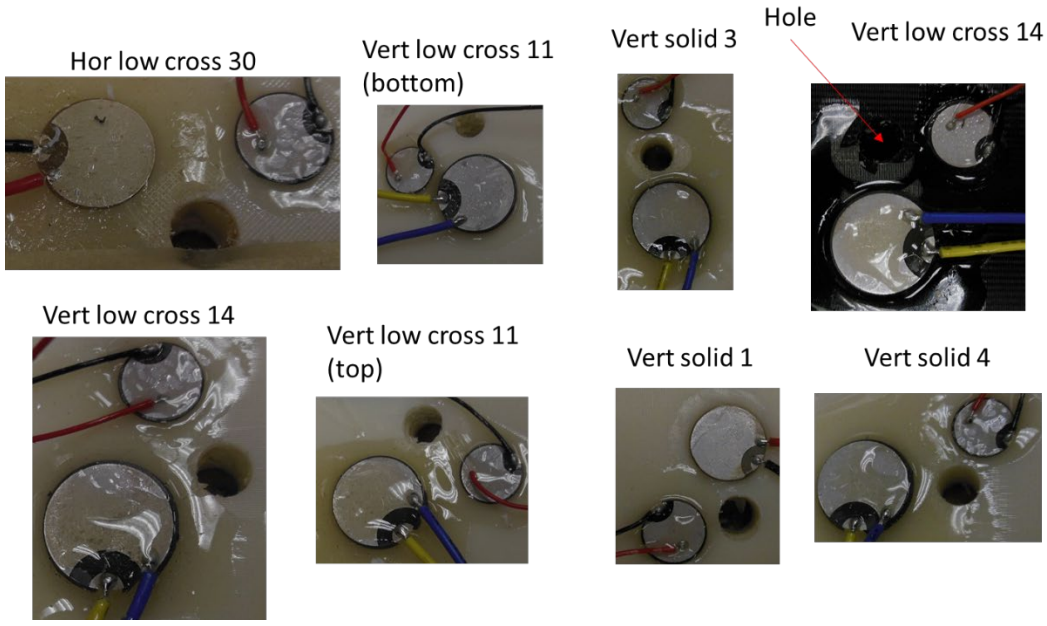

Figure 5.7. The eight samples used for set 4, showing the locations of the drilled holes.

Singular value analysis

The first attempted analysis was based on linear algebra. Sets 1 and 4 contain 85 measurements, and each measurement is a time series of 10,000 points (amplitude and time). Using each measurement as a column vector and stacking columns next to each other gives a 10,000 x 85 matrix. If samples are uniquely identified, then each column should be linearly dependent (in 10,000-dimensional space) to the other 4 measurements taken on the same sample, and linearly independent of any measurement taken on any other sample. One way to test this hypothesis is by taking the singular value decomposition of the matrix, which in this case gives a vector of 85 singular values (plotted in Figure 5.8). If the hypothesis is correct, than only 17 of the 85 singular values will be significant, and the rest negligibly small [1]. Such is not the case, as the values do not fall to zero past index 17. Some other analysis will be needed.

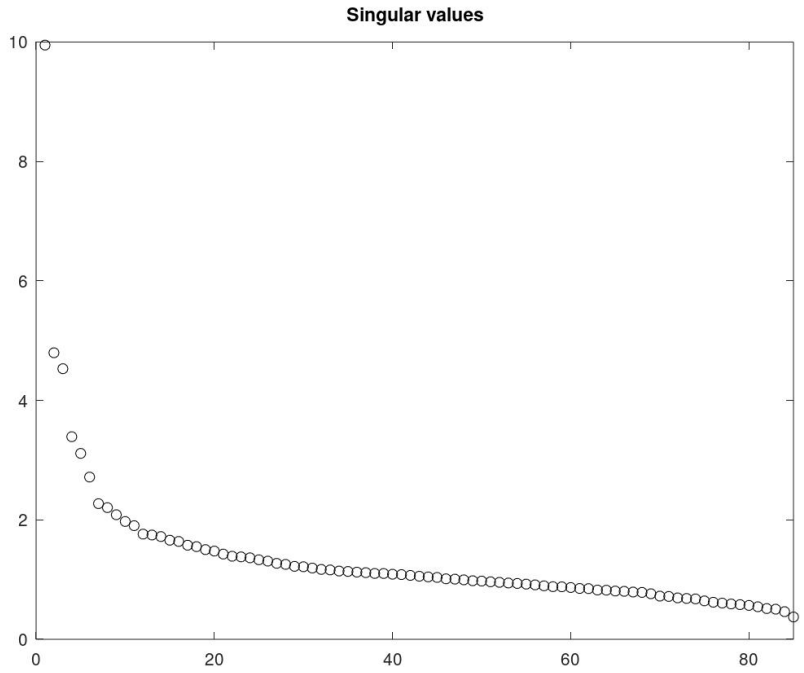

Figure 5.8. The singular values corresponding to the data from sets 1 and 4. The horizontal scale is the index for each value, and the vertical scale is the value itself.

A similar analysis was done on sets 2 and 3, containing 80 measurements. Using each measurement as a column vector and stacking the columns next to each other gives a 10,000 x 80 matrix. If samples are uniquely identifiable, then all but 16 of the singular values for the matrix should be negligibly small. Again, this is not the case (see Figure 5.9), requiring closer inspection.

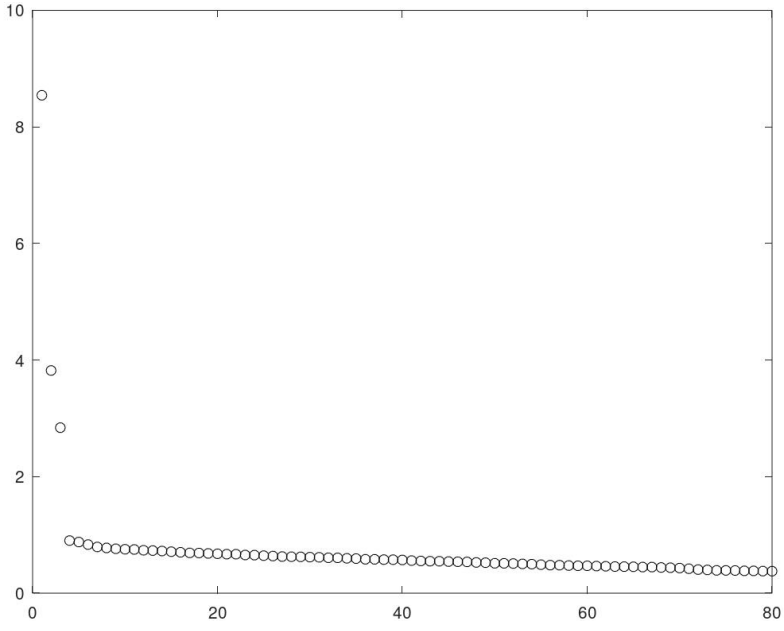

Figure 5.9. The singular values corresponding to the data from sets 2 and 3. The horizontal scale is the index for each value, and the vertical scale is the value itself.

Correlation analysis

A more fruitful approach was to seek the highest cross-correlation between each possible pair of distinct signals. In sets 1 and 4, this means comparing signal 1 against signal 2, signal 1 against signal 3, signal 1 against signal 4, … , signal 1 against signal 85, signal 2 against signal 3, signal 2 against signal 4, … , signal 2 against signal 85, signal 3 against signal 4, … , signal 84 against signal 85. The mapping between TEK files and indices are given in Table 5.1, with sets 1 and 4 treated separately from sets 2 and 3.

If samples are uniquely identified, then the correlation should be higher between two of the five signals from the same sample than between signals from different samples. As an illustration of the method, Figure 5.10 and Figure 5.11 show the raw output voltage data in TEK00001 and TEK00005, respectively.

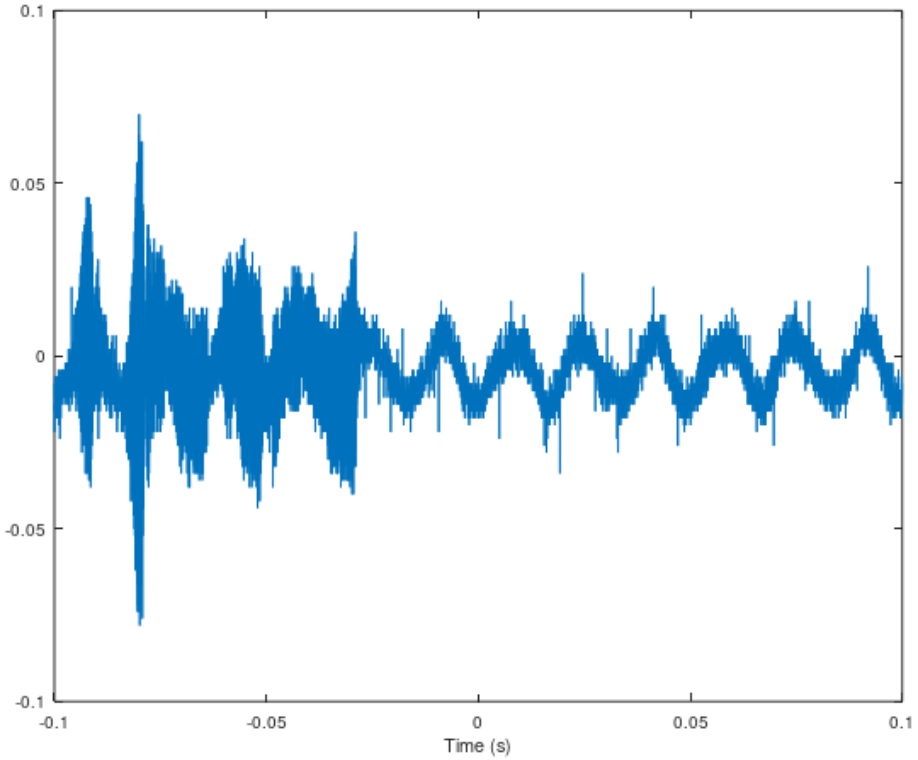

Figure 5.10. Raw voltage data from TEK00001, as a function of time.

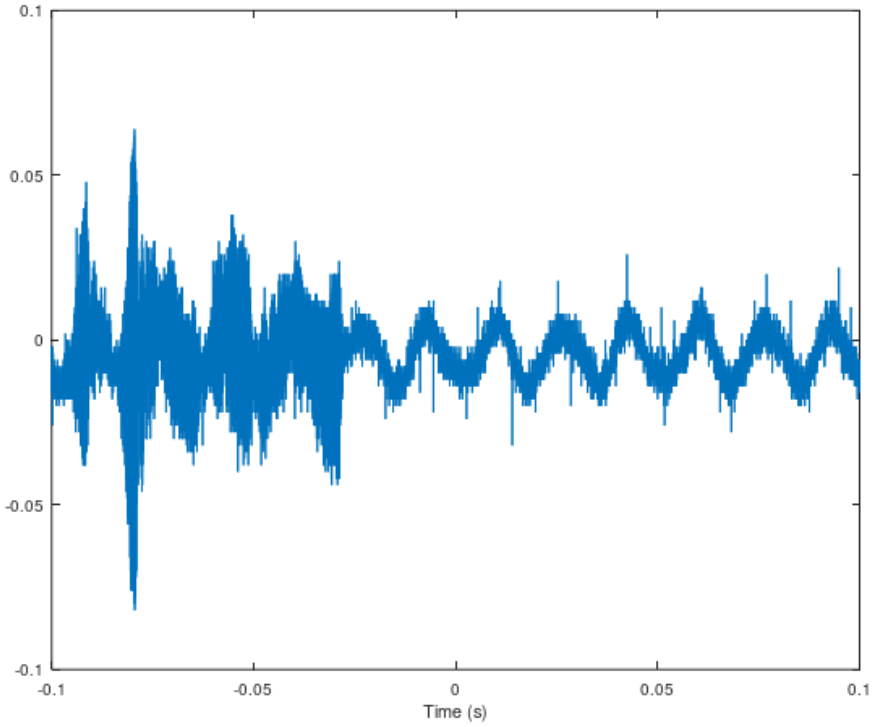

Figure 5.11. Raw voltage data from TEK00005, as a function of time.

The previous two figures display a 60 Hz component which is likely electrical noise into the function generator. Before proceeding with correlation, the signals were put through an 80 Hz sharp-edged high-pass filter with results displayed in Figures 5.12 and 5.13. Notice how these measurements from the same sample have a similar shape in several features, such as the increasing amplitude between -0.04 and -0.03 seconds.

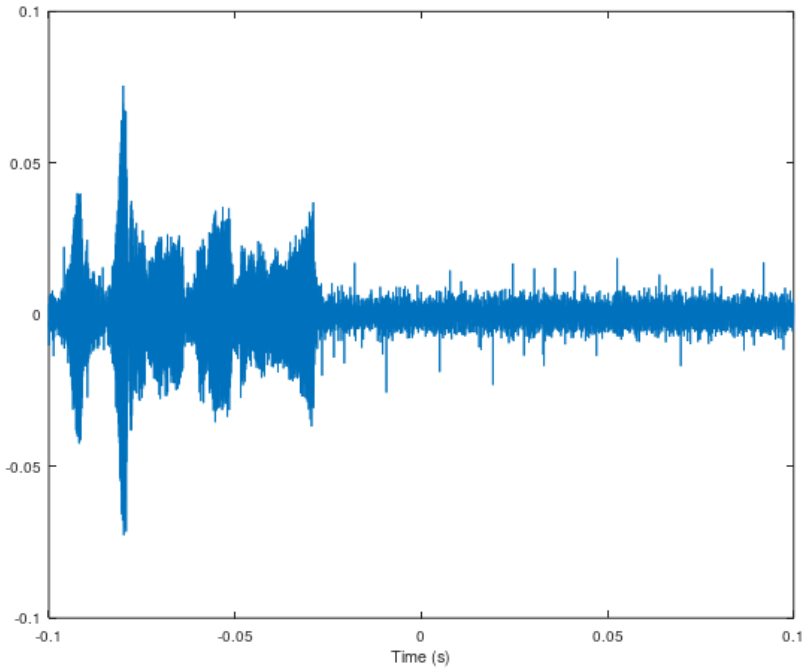

Figure 5.12. Voltage data from TEK00001 after high-pass filtering.

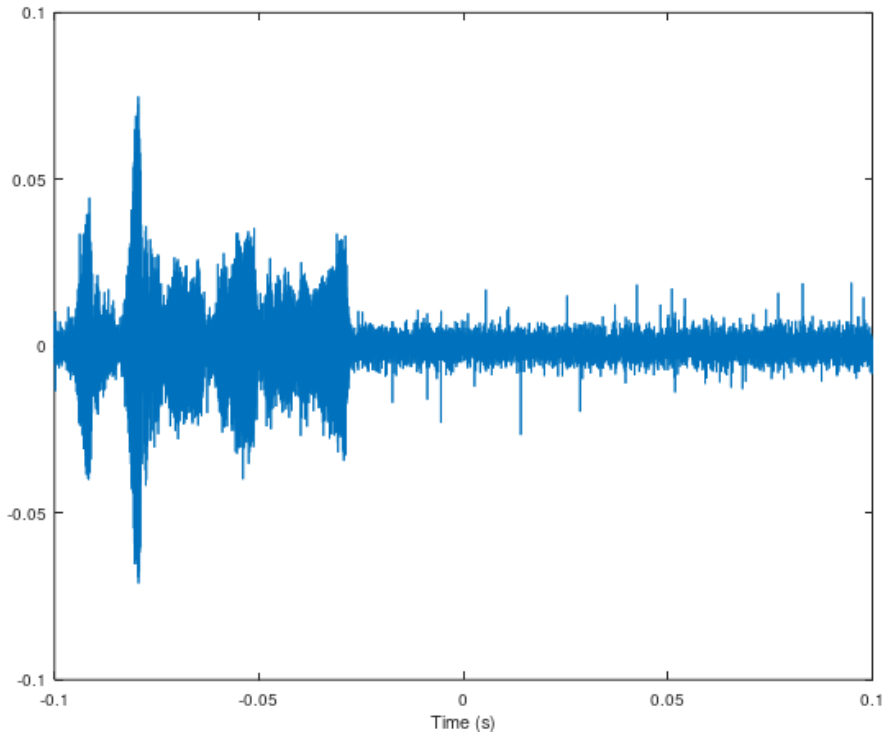

Figure 5.13. Voltage data from TEK00005 after high-pass filtering.

Since the frequency of excitation was as high as 20 kHz, the peaks and troughs of each time series (in this example, TEK00001 and TEK00005) are only a few data points wide. Any synchronization error, where two signals start at different times in the oscilloscope readings, will prevent the peaks of otherwise similar signals from aligning and suggest little cross-correlation even when the responses (started at the same time) are actually correlated. Such synchronization error was difficult to avoid in these tests because noise would trigger the oscilloscope across a range of 0.03 seconds. Therefore, when correlating two signals, we tried translating the second signal against the first by increments of one point. For example, if TEK00005 was translated forwards by 5 points compared to TEK00001, the first 9995 points of TEK00005 would be cross-correlated with the last 9995 points of TEK00001. Conversely, if TEK00005 was translated backwards by 5 points compared to TEK00001, the last 9995 points of TEK00005 would be cross-correlated with the first 9995 points of TEK0001.

This process of translation and correlation was repeated over a range of translations, from 3500 points backwards to 3500 points forwards. Figure 5.14 shows the correlation plotted as a function of translation distance, with positive distance for forward translation and negative distance for backwards translation. The figure shows how sensitive cross-correlation is to translation: only a tiny shift in when the oscilloscope began recording can turn a positive correlation into a zero or negative correlation. However, at the specific translation where TEK00001 and TEK00005 are best aligned, they have a cross-correlation of ~0.8, suggesting that they are very similar responses.

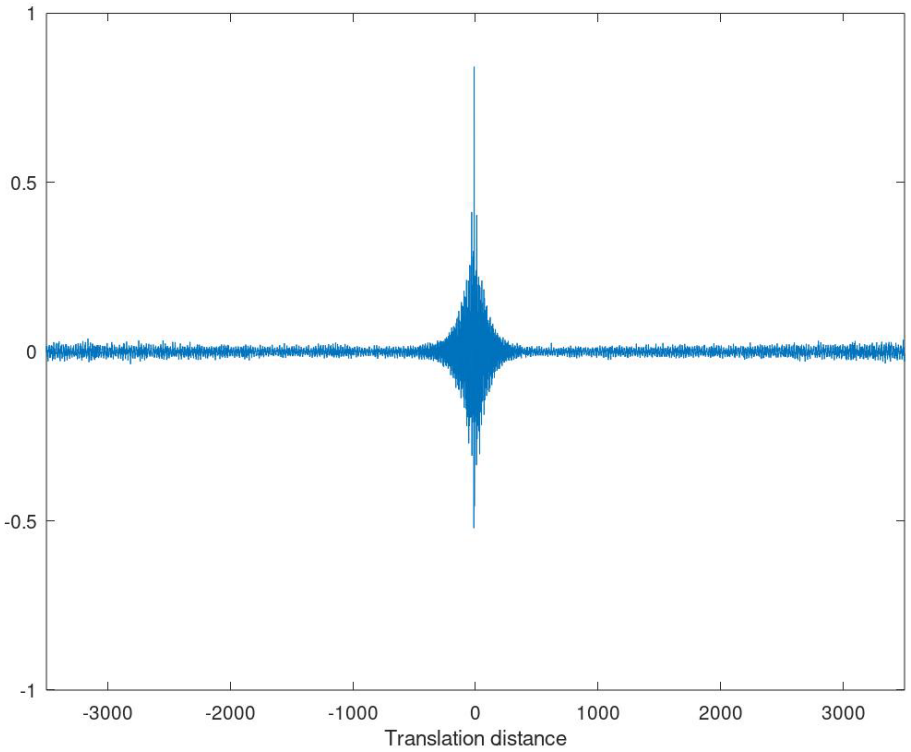

Figure 5.14. The correlation coefficient between TEK00001 and TEK00005 as a function of moving one against the other. Translation distance here is measured in sample units: distance 5 means that the first 9995 points of TEK00001 are compared to the last 9995 points of TEK00005. Distance -5 means that the last 9995 points of TEK00001 are compared to the first 9995 points of TEK00005.

The matching process presented between Figure 5.10 and Figure 5.14 was performed for each pair of samples in sets 1 and 4, and separately for each pair of samples in sets 2 and 3. First, consider sets 1 and 4. The 85 x 85 correlation matrix for all signals is presented in Figure 5.15. Such a matrix is constructed with indices from 1 to 85 (see Table 5.1 under sets 1 and 4) on both the horizontal and vertical axis. Every point (i, j) is colored according to the cross-correlation of measurement i and measurement j, with red indicating high correlation and blue indicating low correlation (all correlations were positive because of translating the measurements to find the maximum value). Elements on the diagonal have the highest possible correlation of 1, because any measurement is perfectly correlated with itself. The matrix is also symmetric across the top left-bottom right diagonal, since the correlation of i with j equals the correlation of j with i. 5 x 5 blocks along the diagonal represent the 5 measurements taken from the same sample; if samples are uniquely identified, then such blocks should be closer to red while the rest of the matrix is closer to blue. For ease of interpretation, the vertical axis is labeled with sample types (groups of indices according to Table 5.1); the horizontal axis from left to right is the same as the vertical axis from top to bottom.

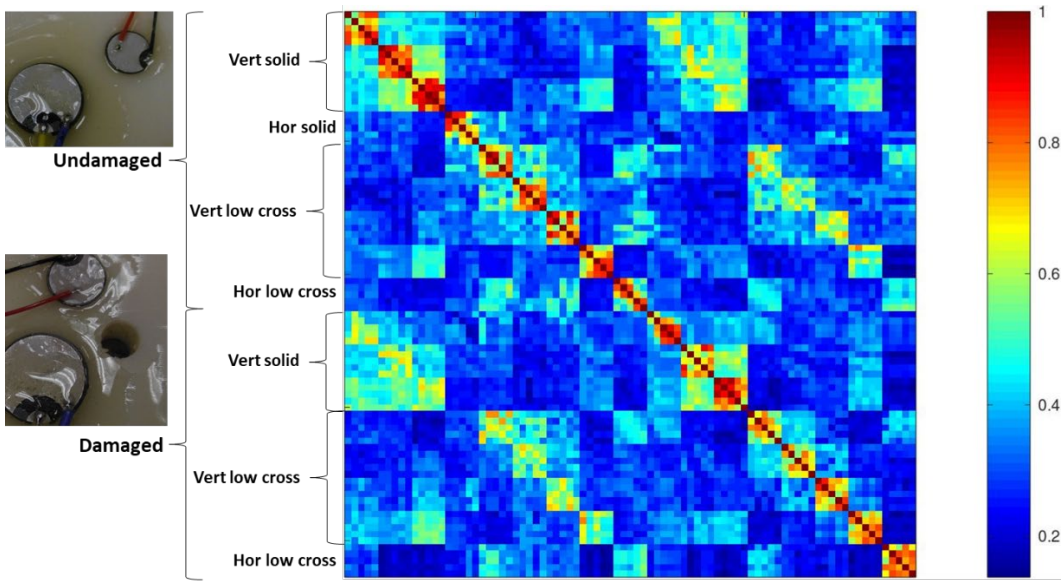

Figure 5.15. The correlation matrix for sets 1 and 4.

The correlation matrix allows us to test samples not just for uniqueness, but also for similarity within categories of several samples having the same construction. The "vertical solid" samples correspond to indices 1 to 15 and 46 to 60 (out of 1 to 85 in total). These rows and columns of the matrix are isolated and displayed separately in Figure 5.16, with the same color axis as the whole matrix. If there are few or no blue squares in Figure 5.16, then "vertical solid" samples are consistently identified with each other compared to the remainder. Of particular interest is whether the analysis method can distinguish samples with drilled holes from samples without. If such damage detection is achieved, then the top right and bottom left sections of the figure should be strongly blue, while the top left and bottom right sections should be consistently closer to red.

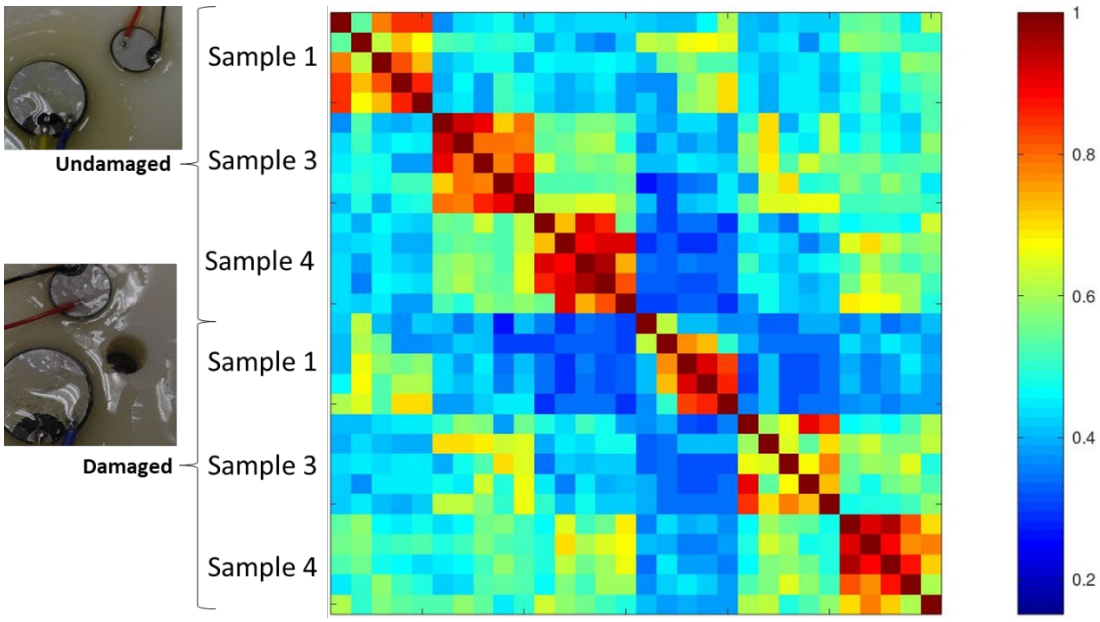

Figure 5.16. The correlation matrix for vertical solid signals.

Likewise, measurements of the "vertical low cross" samples (indices 21 to 40 and 61 to 80) are shown in Figure 5.17. Measurements of the "horizontal low cross 30" sample (indices 41 to 45 and 81 to 85) are shown in Figure 5.18.

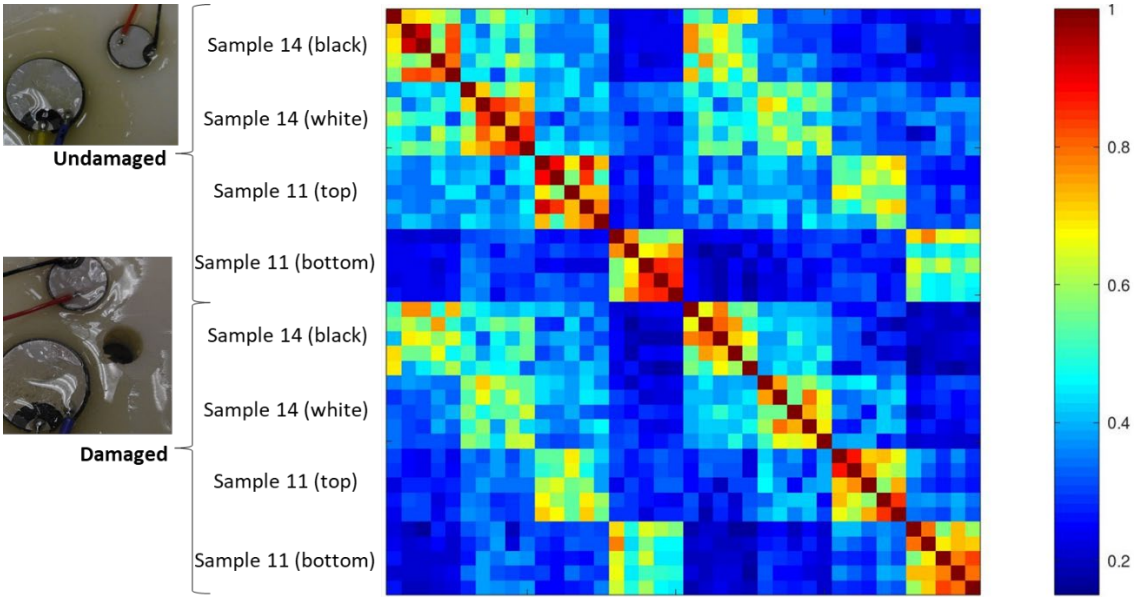

Figure 5.17. The correlation matrix for vertical low cross signals.

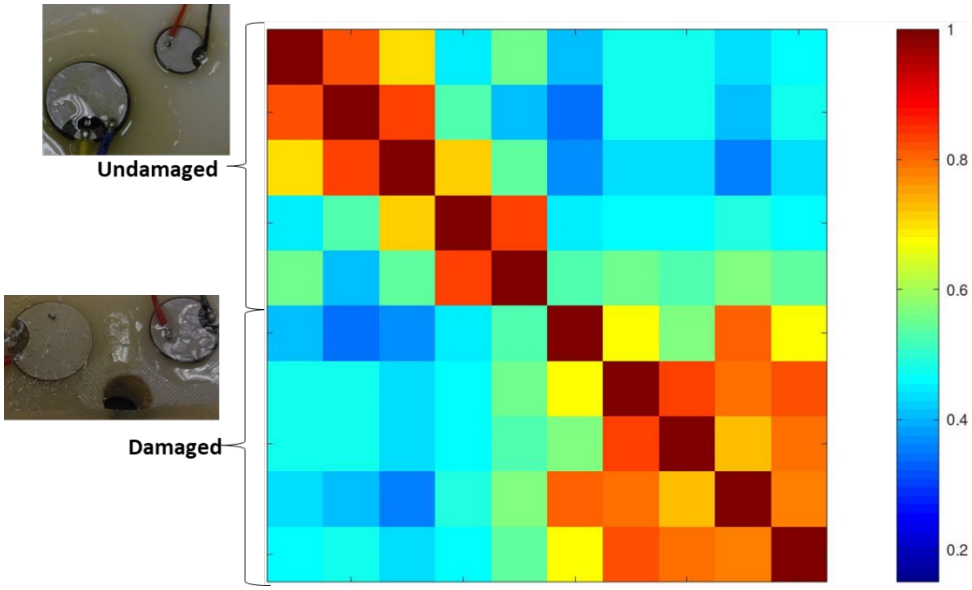

Figure 5.18. The correlation matrix for horizontal low cross 30 signals.

Now consider sets 2 and 3. Because the excitations had to cross the thickness and width of the samples, the output signals were much weaker than for set 1 (see Figure 5.19 by comparison with Figure 5.12 and Figure 5.13).

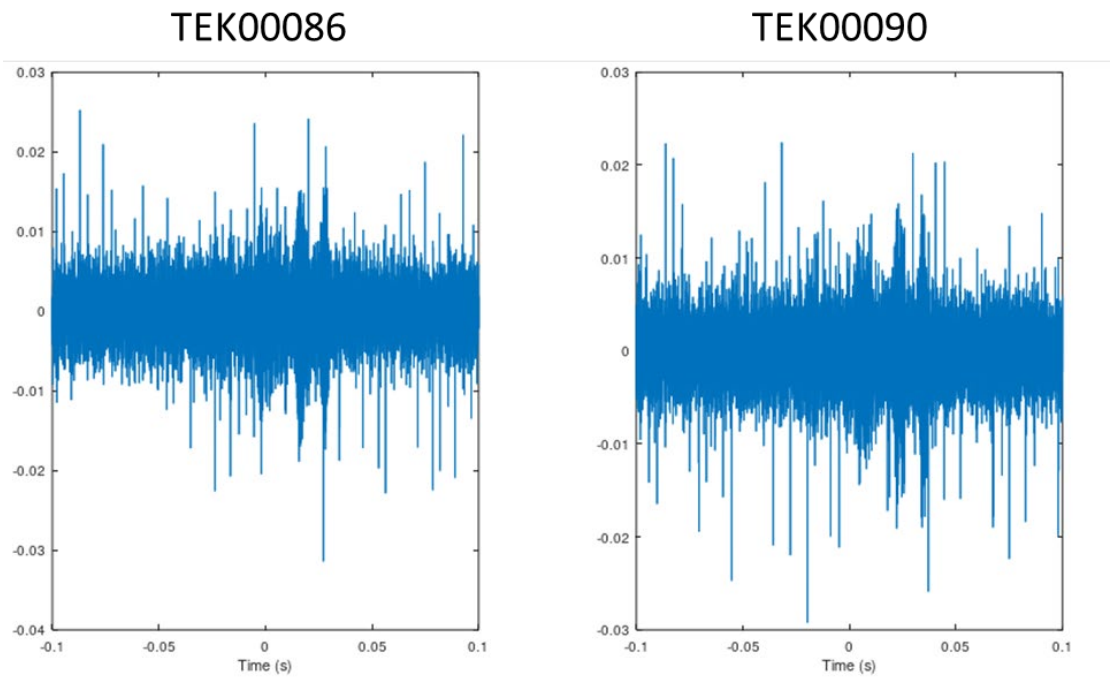

Figure 5.19. Voltage data from TEK00086 and TEK00090 after high-pass filtering.

The correlation matrix for sets 2 and 3 is shown in Figure 5.20. For clarity, the submatrices corresponding to vertical low hex, vertical high hex, vertical high cross and horizontal high cross samples are shown in Figures 5.21 to 5.24, respectively. In general, the hex samples appear to be better distinguished than the cross samples (from the respective remainder of the samples). The damaged measurements are often poorly distinguished from the undamaged measurements.

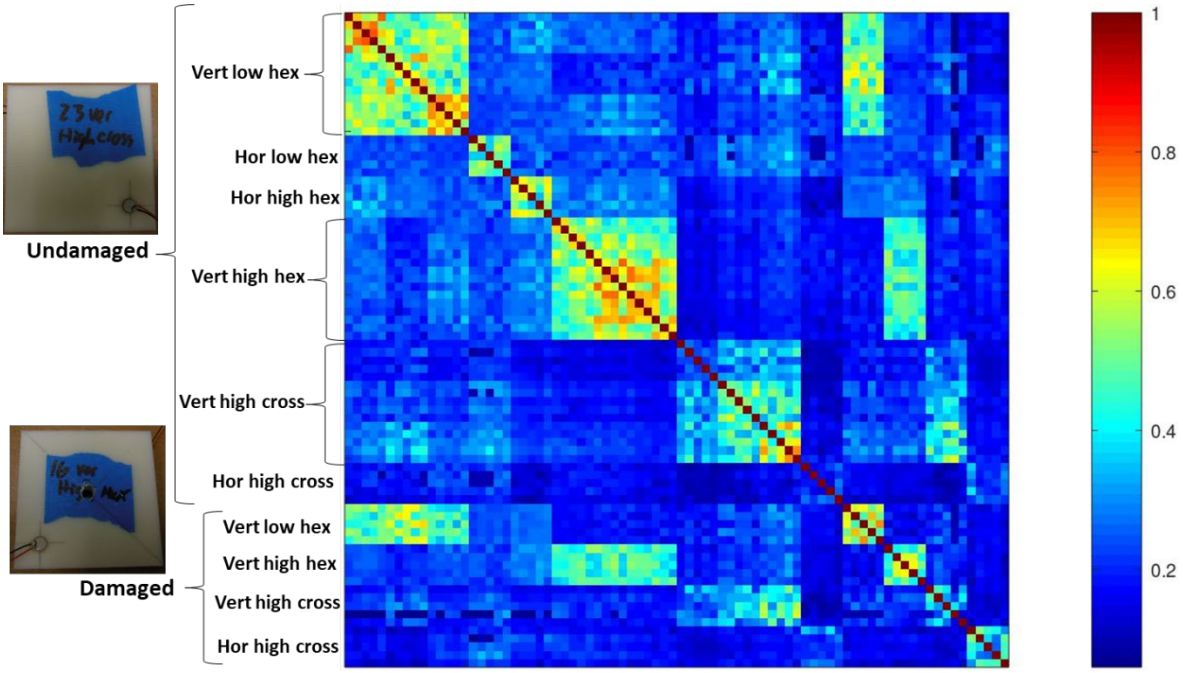

Figure 5.20. Correlation matrix for sets 2 and 3.

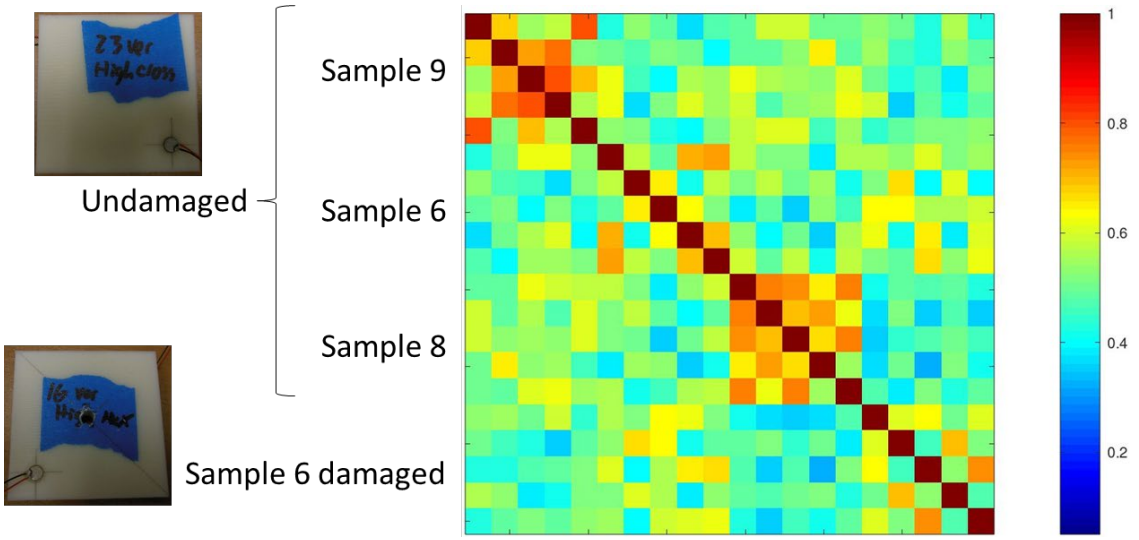

Figure 25.21. Correlation matrix for vertical low hex signals.

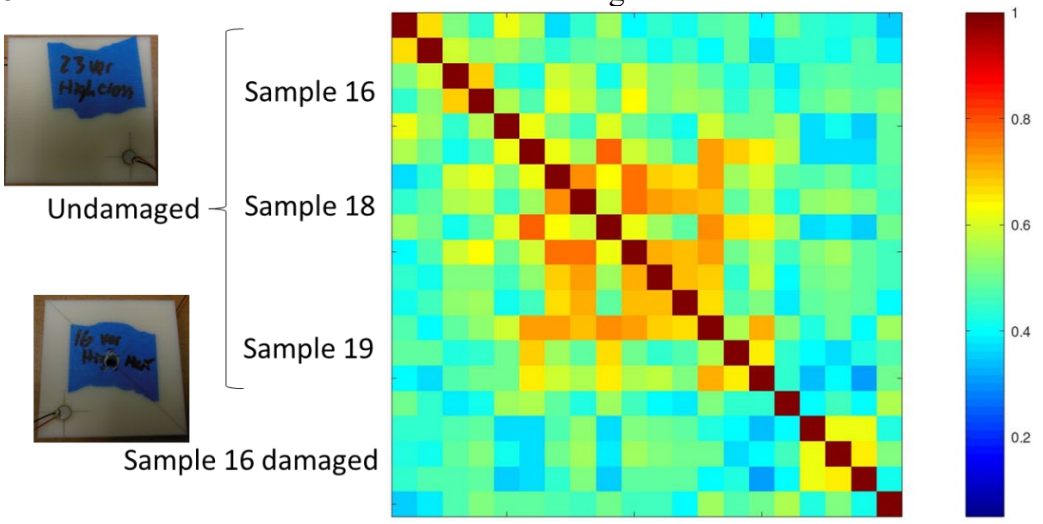

Figure 5.22. Correlation matrix for vertical high hex signals.

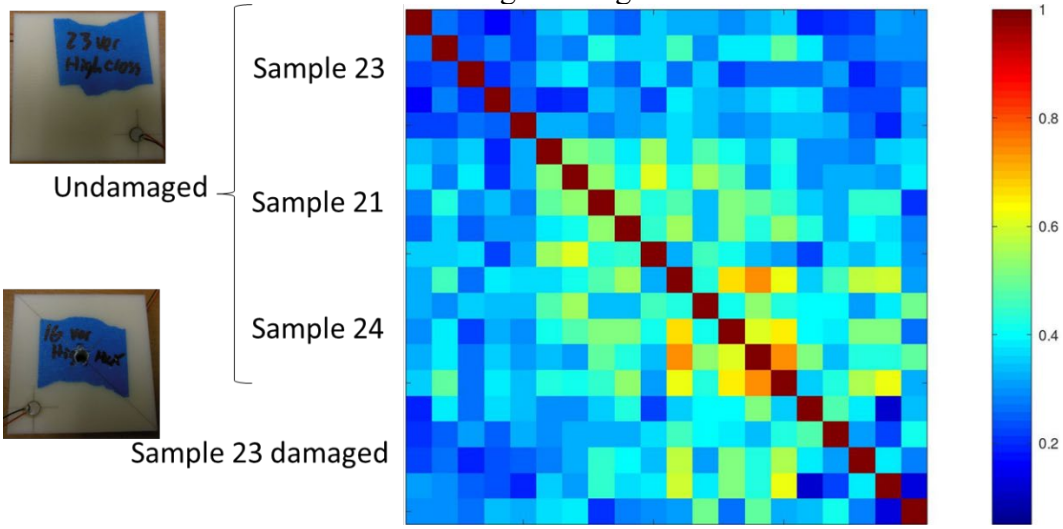

Figure 5.23. Correlation matrix for vertical high cross signals.

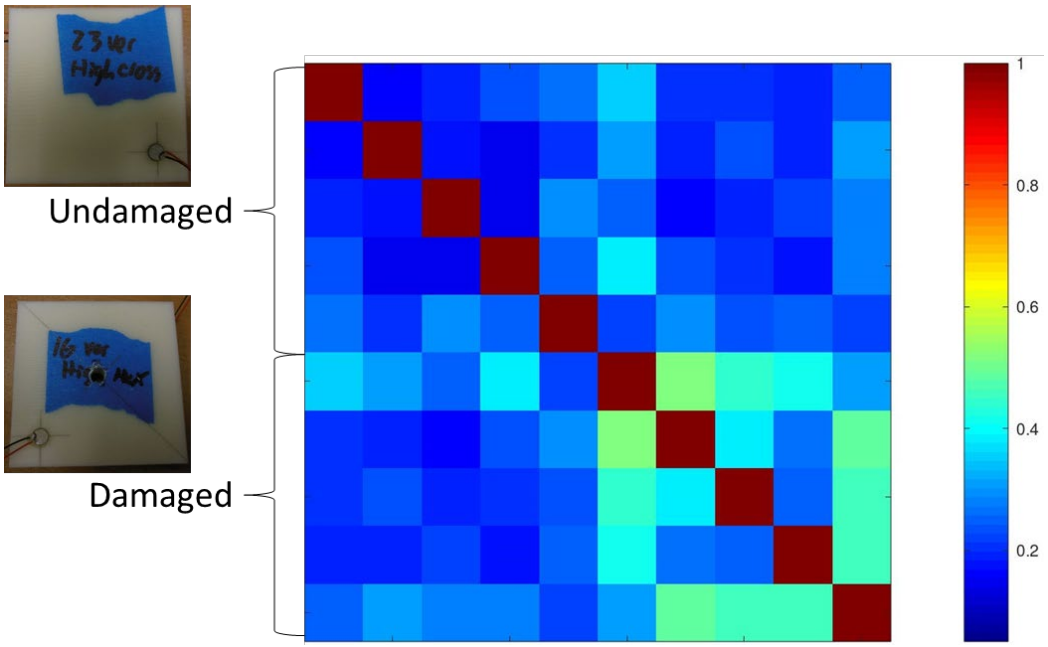

Figure 5.24. Correlation matrix for horizontal high cross 34 signals.

Conclusions:

The first conclusion from these measurements is that categories of coupons, and to a lesser extent individual coupons, are somewhat distinguishable using PZTs in this manner. Sets 1 and 4 in particular have high correlation on the 5 x 5 diagonal blocks for individual coupons (Figure 5.15). The diagonal is less pronounced for sets 2 and 3 (Figure 5.20). On the other hand, most measurements show a high correlation among samples of the same structure compared to samples of different structure. The primary exceptions were that "vertical low cross 11 (bottom)" appears distinctly from the other "vertical low cross" measurements (Figure 5.17), and that "horizontal high cross 34" has relatively low correlations generally (Figure 5.24). In summary, the method used here identifies construction parameters more effectively than individual pieces.

The second conclusion is that the method does a poor job of damage detection. Otherwise, all submatrices should have a pronounced block of blue squares in their top right and bottom left sections, indicating that the drilled hole significantly altered the signal that reached the oscilloscope (i.e. reduced the correlation) compared to before drilling. This only occurred for "horizontal high cross 34," where correlations were low more broadly. Even "vertical solid 3," with a hole directly between the sensors, shows a correlation above 0.6 between many damaged and undamaged measurements, which is not distinguished from comparisons between undamaged measurements on different coupons (Figure 5.16).

Overall, we conclude that the use of PZTs and vibration transmission is unlikely to detect container damage from tampering. Even with holes drilled straight through the ABS coupons near the PZTs, the vibration signals went around the holes in much the same way as if the holes were absent. What the method can more plausibly check is that the container has the internal structure it should have, since correlations were notably high within measurements of the same structure. In this way one might flag containers that deviate from some standard processing, perhaps because the authentic container was discreetly replaced.

Reference

[1] J. Pillow, "Statistical Modeling and Analysis of Neural Data (NEU 560) Lecture 3A notes: SVD and Linear Systems," 3 October 2019. [Online]. Available: http://pillowlab.princeton.edu/teaching/statneuro2018/slides/notes03a_SVDandLinSys.pdf.

6.0 Project Summary

The refined goals of this study were, through the utilization of existing LANL technologies, to design, fabricate, and test two functional tamper evident containers. The first of these containers used additive manufacturing to construct a non-conductive plastic container with embedded electrically conductive traces. An analog circuit was designed to track the integrity of these traces while an encrypted digital processor monitored and recorded the state of health of the container (see Figure 6.1).

A second container (Figure 6.1) used a similar set of technologies but relied on fiber optic traces, embedded in an additively manufactured plastic container, to assess the integrity of the structure. A laser and photodiode were used to pulse the fiber optic cable to assess its continuity. During the integration of the additive manufacturing technologies for the fiber optic embedding, the team developed the method and procedures for embedding fiber optics in additively manufactured plastic parts. This development is being considered for its potential patenting.

A third sensing scheme that utilized mechanical vibration propagation was explored but inconsistent sensing results along with finite time and resources prevented the team from building a demonstration unit of that technology.

All-in-all, the goals of this technology demonstration project were met and the TEC demonstration units are now available to showcase these technologies to prospective customers and programs.

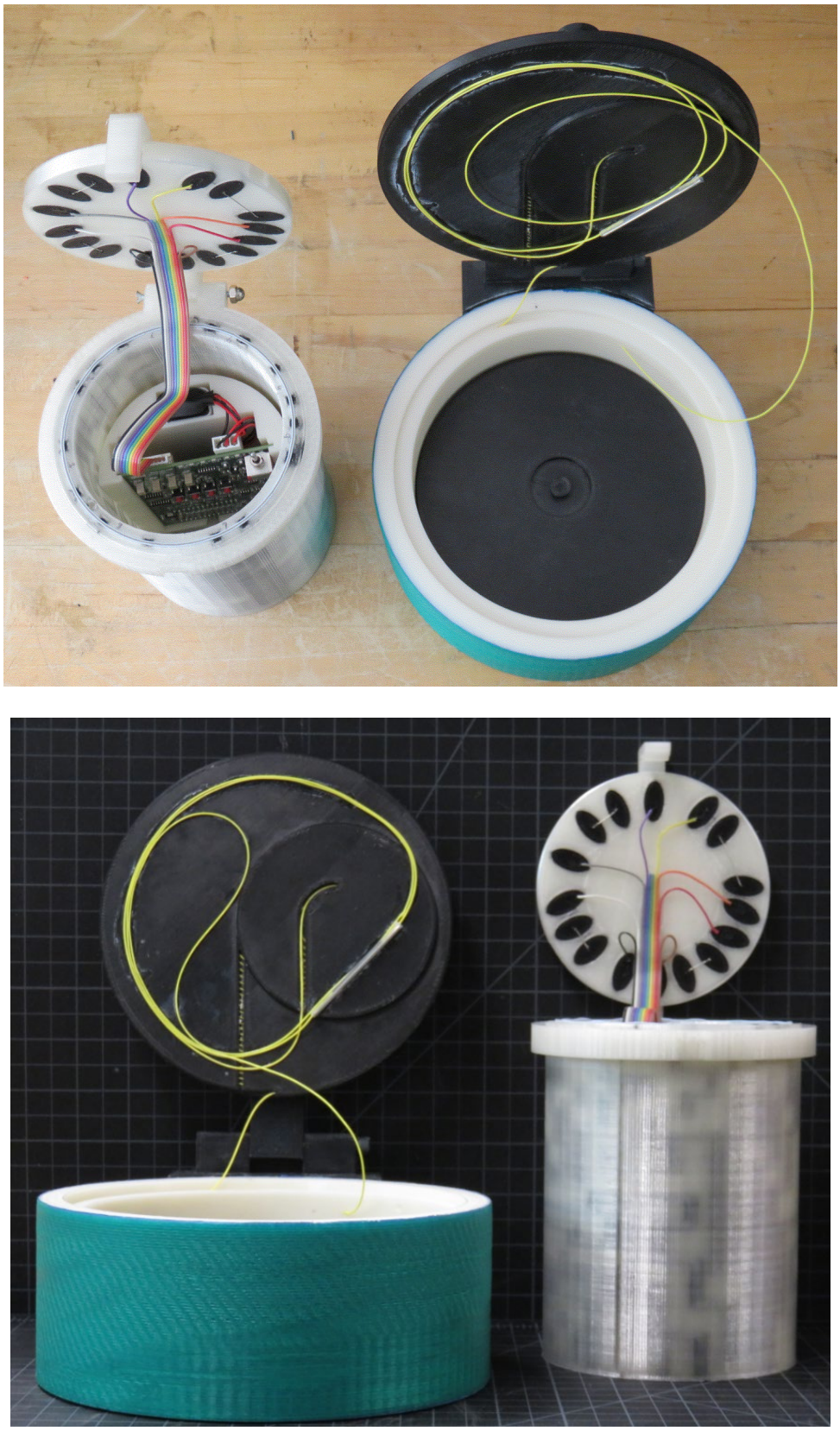

Figure 6.1. CT TEC and FOC TEC demonstration units.